Modeling and Simulation of the Cooling System in Heavy Duty Trucks

Edward Ekstedt

LUND UNIVERSITY

Department of Automatic Control

MSc Thesis
TFRT-6021
ISSN 0280-5316

Department of Automatic Control
Lund University
Box 118
SE-221 00 LUND
Sweden

Printed in Sweden by Tryckeriet i E-huset
Lund 2016

Abstract

This MSc thesis covers the development of a Modelica model of an engine liquid cooling system for the trucks manufactured by MAN Truck & Bus AG. The mathematical assumptions used for transcribing existing models are described and the reasoning behind the modeling process is provided.

The separate component models are validated with two sets of input signals. Primarily with a dynamic, transient cycle recorded at a testing track. Secondarily, they are also validated with steady state measurements which were part of an experiment conducted at MAN's test bench.

Furthermore, the modeling process of the heat exchanger stack at the front of the vehicle is presented together with points about the boundary conditions of the cooling air. These components are then integrated with each other in a model of the entire cooling system, yielding acceptable simulation results.

Additionally, the simulation performance is evaluated and different integration algorithms are compared and tested, to investigate the possibility of applying the model to real time interfaces. It shows that the model is stable for fixed-step algorithms with small enough step sizes, and that HIL-simulation is possible.

Preface

The project was carried out at MAN Truck & Bus AG, the team within Engineering Research Vehicle Dynamics & Simulation Technology for *Powertrain Dynamics & Thermal Management*, in Munich, Germany, during the months of March to August, 2016. It was carried out at the request of MAN Truck & Bus AG and Modelon AB.

I want to express my gratitude to the people who assisted me in the project, especially to Dr. Michael Bernath, my supervisor at MAN Truck & Bus AG, Daniel Andersson, my supervisor at Modelon AB, and Karl-Erik Årzen and Olof Troeng, my supervisors at the Department of Automatic Control, Lund University.

Additionally, I would like to thank some other individuals at MAN Truck & Bus AG who assisted me with the following subjects, Dr. Robert Höpler, who assisted with FMI, optimization, and HIL-simulation, Jan Swoboda, who assisted with thermodynamics, and Fabian Schweizer, who assisted with HIL-simulation.

Contents

Fluid Dynamics and Thermodynamic Notations

Parameter	Description	Unit
C_d	Discharge coefficient	[1]
c_p	Specific isobaric heat capacity	$[\mathrm{J}/(\mathrm{kg\,K})]$
D	Hydraulic Diameter	[m]
k	Thermal conductivity	$[\mathrm{W}/(\mathrm{m\,K})]$
$\dot{m}$	Mass flow rate	[kg/s]
n	Rotational speed	[1/s]
NTU	Number of transfer units	[1]
p_{in}	Inlet pressure	[Pa]
p_{out}	Outlet pressure	[Pa]
$\dot{Q}$	Heat transfer rate	[W]
$\dot{Q}_{max}$	Maximum heat transfer rate	[W]
$T_{h,i}$	Inlet temperature, hot side	[K]
$T_{c,i}$	Inlet temperature, cold side	[K]
$T_{h,o}$	Outlet temperature, hot side	[K]
$T_{c,o}$	Outlet temperature, cold side	[K]
UA	Overall heat transfer coefficient	[W/K]
$\dot{V}$	Volume flow rate	$[\mathrm{m}^3/\mathrm{s}]$
ε	Effectivity	[1]
ρ	Density	$[\mathrm{kg}/\mathrm{m}^3]$
ζ	Friction coefficient	[1]

1

Introduction

1.1 Background

Vehicle manufacturers have increasing demands on low fuel consumption, both from the consumers and from legislation over the world. Dynamic simulation models of the physical systems in the vehicle and how these systems interact with each other help the manufacturers to optimize the fuel consumption by improving the design and control. In order for these models to be successful, they must be fast, stable and accurate.

MAN Truck & Bus AG, hereinafter referred to as MAN, is an international company based in Munich, Germany. As a manufacturer of commercial vehicles, they strive to improve their models which describes the system in their vehicles and components. As such, they have requested the development of a Modelica model of the engine liquid cooling system in their Euro VI truck series. The model should be developed by utilizing Modelon's Liquid Cooling Library[1] for Dymola, and be possible to implement in real time systems.

1.2 Purpose

The purpose of this master's thesis is to develop a Modelica model in Dymola of the cooling circuit of one of MAN's long haul truck engines. The aim of the model is to help MAN achieve fast and accurate simulations, with the possibility of the models being utilized in real time control. The model should contain the entire cooling cycle, split between the low and the high temperature cycles. The coolant pump, heat exchanger stack, and low and high pressure charge air coolers are examples of components that should be modeled.

[1] A Dymola library is a commercial package of models

A mock up block schedule of the model implementation is shown in Figure 1.1. The model's boundary conditions are delivered from the trucks internal computer to the model. The boundary conditions include fan and pump rotational speeds. The model then simulates the coolant cycle for the given boundary conditions, and delivers this data to a predictive control module. Together with the measurement data, the predictive control module should predict the necessary control signals, e.g. fan and pump rotational speed, and return these to the truck internal computer and the Dymola model. The end goal is to reduce fuel consumption, which is achieved by limiting the power used by the components in the system.

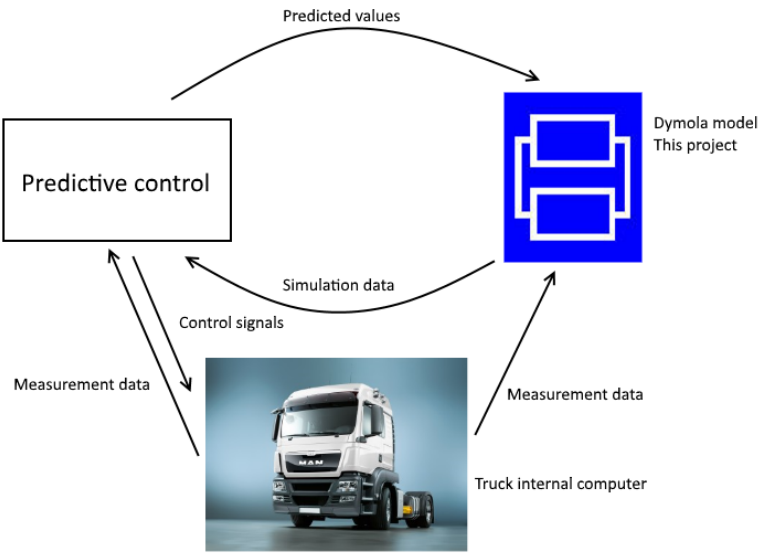

Figure 1.1: Mock up block schedule of the connections between the model, the truck, and the planned predictive control.

1.3 Related work

Modelica The reasoning and aim of the creation of the Modelica language was discussed by Elmqvist and Mattsson in 1997 [4], and has since been applied in a wide range of subjects.

Thermo-hydraulic systems The creation of a base library in Modelica for thermo-hydraulic systems was proposed by Tummesheit et al. in 2000, [14], where they also describe the concept of volume and flow models.

Vehicle thermal management Batteh et al. described how to model vehicle thermal management using Modelon libraries in 2014 [1]. The cooling system in the vehicle is modeled with Liquid Cooling Library. [9]

Earlier Models Jan Swoboda at MAN has created a model in GT-SUITE. The technical data regarding the components in the cycle was retrieved from this model. GT-SUITE is a modeling software created by Gamma Technologies. The modeling is complex and contains a complete model of the cooling cycle, including the combustion engine and turbochargers. The complex model leads to slow simulation times and is not suited for real time applications.

Previous modeling and projects on liquid cooling modeling has not been studied extensively. The basis of the liquid cooling modeling has been acquired from courses given at Modelon AB concerning thermofluid modeling.

1.4 Liquid Cooling Library

Liquid Cooling Library, further on referred to as LCL, is a commercial library for Dymola created and distributed by Modelon AB.

In large, the library contains two different components, *flow* components and *volume* components. In flow components, the pressure in the ports is processed to compute mass flow rate. In volume components, dynamic mass and energy balances are applied and the continuous time fluid properties such as enthalpy, pressure, and mass fraction are used to connect two different components. These types of components should be alternated to increase model stability.

The liquid models in LCL are incompressible, meaning that the liquid density is independent of the pressure, volume components have quasi-static mass balances and the liquid specific enthalpy is independent of pressure. The data describing the coolant is retrieved from the International Institute of Refrigeration. [11]

The gas models, however, are modeled as compressible and thus more sensitive to erroneous modeling. It is imperative that that the alternation of volume and flow

components is applied when working with the compressible gas models, as otherwise the simulation easily fails. The air model used is provided by NASA. [10]

Furthermore, most LCL components have the parameter option of deciding whether the mass flow rate is a function of the pressure drop or vice versa. This gives the freedom of choosing which boundary conditions are present in the model, and may be used to further validate a model [9].

1.5 Limitations

Creating a proper model of the heat flow from the combustion engine to the coolant was deemed too difficult with the available tools and libraries. The model was simplified by imposing the measured temperature of the coolant after the engine, as a boundary condition. Furthermore, the heat exchanger properties of the retarder and the oil cooler were not readily available, and were as such replaced with imposed temperatures as well.

The turbochargers were not modeled in Dymola, as the focus of the modeling was on the coolant circuit, rather than the charge air.

1.6 Measurement data

In the modeling process, two sets of measurement data were used. The first and most used set consisted of a transient cycle lasting for 3516.05 seconds, with a sample time of 0.05 seconds, yielding 70322 samples. The transient cycle is a real world testing track, for MAN in Germany. The cycle is varied in velocity and elevation, while keeping the components of the cooling cycle in their respective areas of operation. The velocity of the cycle is shown in Figure 1.2.

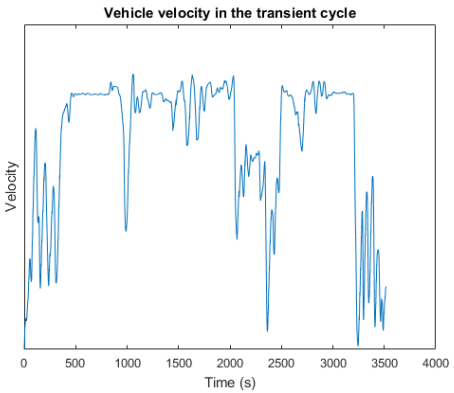

Figure 1.2: Velocity of the vehicle in the transient cycle

The second set is a series of steady state points from an experiment conducted at MAN's test bench. The measurement data is noisy, but post processing yielded 71 steady state points which could be used for the modeling.

A common denominator of the input signal sets is that some of the signals, e.g. temperature and pressure, were measured by sensors in the cycle, and others, such as the mass flow rate, were computed from the measurement data. This led to the consequence that if a sensor was faulty, the error propagated to other variables.

In general, the following signals were used

Temperature In the component models, the temperature values were used as boundary conditions. In both the component and closed circuit models, temperature was used to validate that the temperature changes in the cycle were accurately predicted by the model.

Pressure The absolute pressure of the coolant and air were used as boundary conditions in the open loop, and validation of the pressure drop correlation in both the open and closed loop.

Mass flow rate The mass flow rate of the coolants were used as boundary conditions in the component models, and validation in closed circuit models. The air mass flow rate was used as boundary condition in both closed circuit models and component models.

Heat flow rate The heat flow rates were used as validation for the heat exchanger models.

Rotational speed The rotational speed of the coolant pump and the air fan were used as set inputs for these components.

1.7 Outline of the Thesis

Chapter 2 - Modeling This chapter presents the modeling techniques applied in Dymola and some mathematical models and equations needed to implement the model from existing data.

Chapter 3 - Implementation This chapter covers the validation method, optimization, solver options and the HIL implementation.

Chapter 4 - Results The results of the different modeling approaches and simulations are presented in this chapter.

Chapter 5 - Discussion Discussion of the results is covered in this chapter.

Chapter 6 - Conclusions and Future Work This final chapter covers the conclusions based on the results and discussions and establishes a foundation for future work on the subject.

2

Modeling the Liquid Cooling System

2.1 Cooling System

An image of a MAN Euro VI truck engine is displayed in figure 2.1. One of the main goals of the project was to model this physical system.

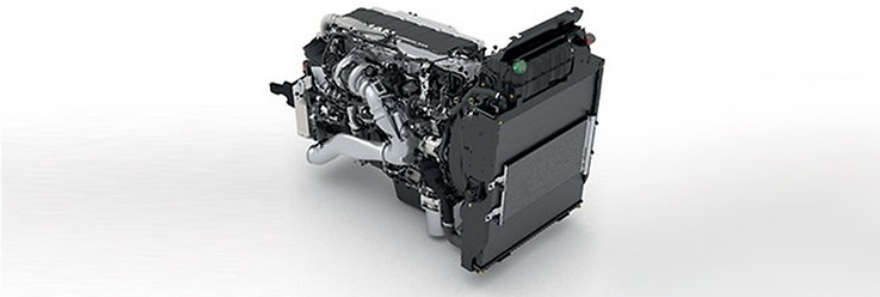

Figure 2.1: MAN Euro VI truck engine. (Source: man.eu)

A schematic of the cooling cycle is shown in Figure 2.2. The cooling system for the engine consists of two interconnected coolant circuits, the high temperature and the low temperature circuits. In the figure, the high temperature cycle has a red color and is labeled (a). The low temperature cycle has a pink and blue color and is labeled (b). The purpose of the low temperature cycle is to cool the charge air provided to the engine. The purpose of the high temperature cycle is to cool the internal combustion engine. The flow in both branches are governed by the coolant pump (2), which is driven by a V-belt from the crankshaft. Right after the pump, the branching occurs.

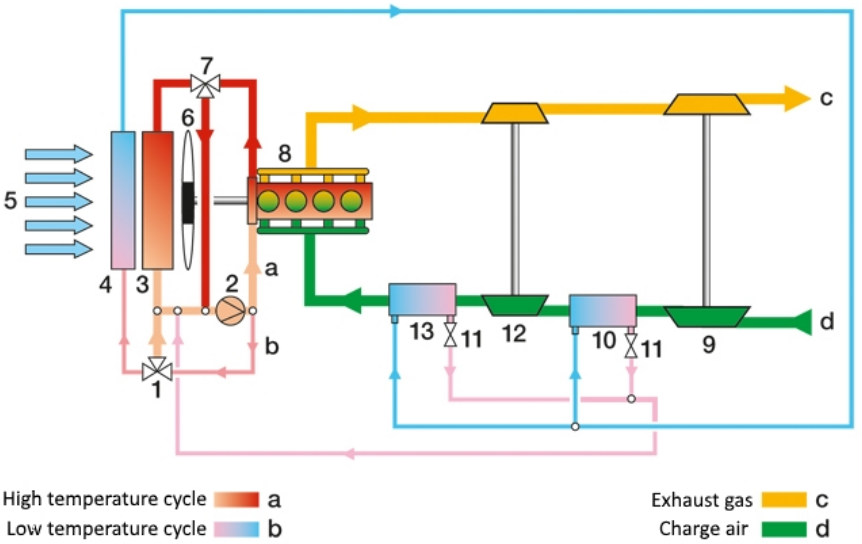

Figure 2.2: The cooling cycle [5]

Table 2.1: Legend for Figure 2.2

Number	Component
1	Pressure relief valve
2	Coolant pump
3	High temperature cooler
4	Low temperature cooler
5	Headwind
6	Viscous fan
7	Main thermostatic valve
8	Internal combustion engine
9	Low pressure turbocharger
10	Low pressure charge air cooler
11	Charge air cooler thermostatic valves
12	High pressure turbocharger
13	Low pressure charge air cooler

Low temperature circuit The coolant flows by the pressure relief valve (1), which protects the circuit if the pressure is too large. If that occurs, the flow is redirected to the pump again. It then goes to the low temperature cooler (4), which is a flat tube heat exchanger, where it gets cooled by the headwind (5). The flow is then branched again between the low pressure charge air cooler (10) and the high pressure charge air cooler (11). As the name suggests, these heat exchangers cool the charge air (d), whose temperature has been increased as a side effect of the pressure increase in the turbochargers (9,12). After the coolers, the flows pass through thermostatic valves (13), one after each cooler, before returning to the coolant pump.

High temperature circuit In the high temperature circuit, the coolant flows from the pump to the engine (8), where it is heated by the excess energy from the combustion. It is then routed through the retarder, a component which helps braking, not pictured, and the exhaust gas recirculation module (not pictured), before arriving at the main thermostatic valve (7). If the temperature is high enough, the flow is directed to the high temperature cooler (3), if it is not high enough, the flow is routed back to the coolant pump. The high temperature cooler is situated right behind the low temperature cooler, utilizing the slightly hotter headwind exhausted by it. The headwind's mass flow rate is increased by a fan (6), driven by a viscous clutch connected to the crank shaft. This clutch is an actuator and can be controlled by the internal computer of the vehicle. The coolant flow is then once again returned to the coolant pump. [5]

2.2 Physical Structure of the Model

The modeling process was divided into three separate processes, single component test benches, multi component cycle test benches, and finally, the closed circuit model. The test benches consisted of few components with strict boundary conditions to ensure that the separate components were correctly modeled.

2.2.1 Test benches

The general outline of the single component test benches were constructed similarly. Most components had two boundary points for the coolant flow. These were the source, in which the temperature and mass flow rate were prescribed by the input signals, and the sink, in which the pressure was prescribed by the input signal. The air-liquid heat exchanger component test benches also included corresponding sources and sinks for the air. An example of the test benches is found in Figure 2.3. It contains the air inlet boundary (1), air outlet boundary (2), coolant inlet boundary (3), coolant outlet boundary (4), heat exchanger model (5), and thermostatic valve (6). External inputs are displayed

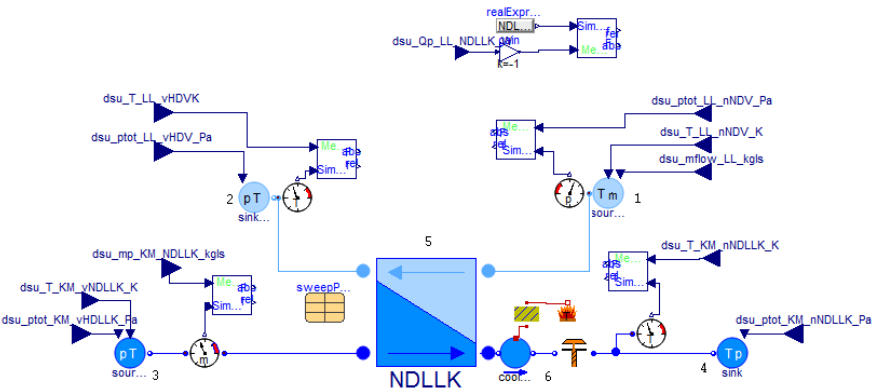

Figure 2.3: Dymola model of the low pressure charge air cooler test bench.

2.2.2 Multi component cycle test bench

After modeling the components separately, combining them into cycle models was the next logical step. The coupling of models led to a number of obstacles, most prominent were the handling of flow branching and multiple boundary conditions. If the model was not properly parametrized, conflicting boundary conditions led to numerical instability and slow simulation speed. One thing to note is the importance of alternating *flow* and *volume* components when using LCL. Doing so will reduce

the sizes of the nonlinear system that the algorithm has to solve at every time step and as such reduces the total computing time needed.

Heat exchanger stack The heat exchanger stack is positioned at the front of the vehicle, and consists of the high temperature cooler and the low temperature cooler. They are both flat tube heat exchangers of the same size. The difference though is that the low temperature cooler is divided into two passes, in which the coolant flows in order, while the high temperature cooler is single pass. The low temperature cooler was discretized into two separate cooler models to represent the two pass dynamics.

2.2.3 Closed circuit

The final modeling task in Dymola was to create a closed circuit model spanning the entire cooling cycle. This implies that there are no boundary conditions for the coolant cycle, with the flow governed by the pump model and the absolute pressure level initialized by a expansion volume component, to add compressibility. This was by far the most time consuming part of the project, since small changes in one component could propagate into the entire model, and initial guess values of the states had large impact. A sample image of the model is found in Figure 2.4, in this picture, the model structure and coloring is based on the model provided by MAN, recall Figure 2.2. The visual clutter is due to multiple vents in the high temperature circuit that are not present in the schematic.

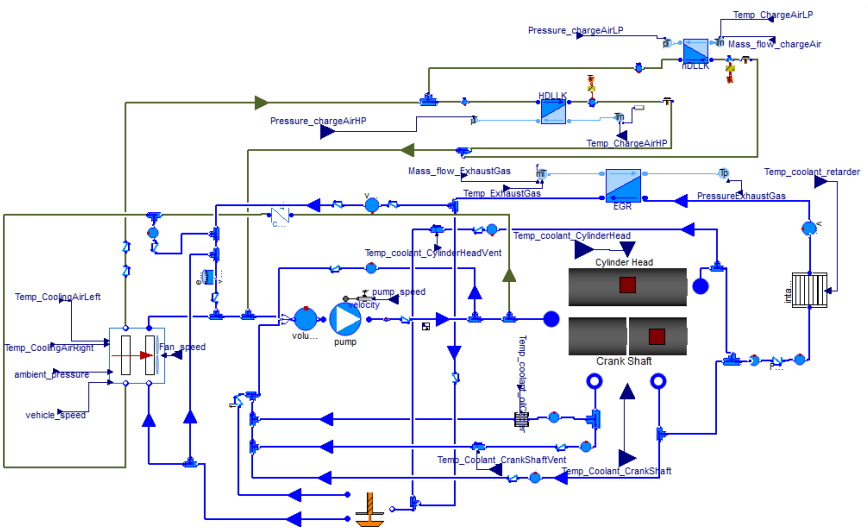

Figure 2.4: A model of the entire cooling cycle in Dymola.

2.3 Mathematical Modeling

2.3.1 Translating from GT

In general, the components in GT-Suite were detailed, containing geometrical, frictional, and thermodynamical data. The base component models in Dymola usually have less parametrization options, to enable faster simulation speeds while retaining the base dynamics and properties. To deal with this, some translations between the simulation tools had to be made to implement the models. Below, the translation processes for friction models and heat transfer models are described.

Friction A pressure drop correlation can be formulated as

$$\Delta p = f\frac{L}{D}\rho\frac{v^2}{2} \quad [\text{Pa}] \tag{2.1}$$

where f is the friction coefficient, L is the pipe or passage length (m), D is the pipe diameter or the hydraulic diameter (m), and v is the mean flow velocity. [12] This correlation is commonly used to analyze pressure drop since it is relatively independent of pipe dimensions and fluid properties. Introducing ζ as

$$\zeta = f\frac{L}{D} \tag{2.2}$$

and substituting in 2.1 we arrive at a correlation used in Liquid Cooling Library,

$$\Delta p = \zeta\rho\frac{v^2}{2}. \tag{2.3}$$

In GT-Suite, the pressure drop correlation is defined as

$$C_d A = \frac{\dot{m}}{\sqrt{\rho 2\Delta p}} \tag{2.4}$$

where C_d is the discharge coefficient and A is the flow area. The correlation between mass flow rate and velocity is

$$\frac{\dot{m}}{\rho}\frac{1}{A} = v, \quad \left[\frac{\text{kg}}{\text{s}}\cdot\frac{\text{m}^3}{\text{kg}}\cdot\frac{1}{\text{m}^2} = \frac{\text{m}}{\text{s}}\right]. \tag{2.5}$$

Substituting $\dot{m}$ in 2.4 yields

$$
\begin{aligned}
C_d A &= \frac{v\rho A}{\sqrt{\rho 2\Delta p}} \\
C_d &= \frac{v\sqrt{\rho}}{\sqrt{2\Delta p}} \\
C_d^2 &= \frac{v^2\rho}{2\Delta p} \\
\Delta p &= \frac{1}{C_d^2}\rho\frac{v^2}{2}
\end{aligned} \tag{2.6}
$$

and thus, by comparing Equations 2.3 and 2.6 we can see that the relation between the friction coefficient ζ in Dymola and discharge coefficient C_d in GT-Suite is

$$\zeta = \frac{1}{C_d^2}. \tag{2.7}$$

As such, translating these pressure drop components was trivial. Other parametrizations of pressure loss were quadratic functions of pressure drop over mass flow rate, or tables with friction coefficient vs Reynolds number. These parametrizations were readily available in Dymola and as such could be transferred without any difficulty.

Heat transfer The methods of computing the heat transfer rate in heat exchangers in LCL are the Effectiveness Method, and Number of Transfer Units (NTU) method. The effectiveness is defined as

$$\varepsilon \equiv \frac{\dot{Q}}{\dot{Q}_{max}}, \tag{2.8}$$

i.e., the ratio of the actual heat transfer rate to the maximum possible heat transfer rate of the heat exchanger. [2]

$\dot{Q}_{max}$ is defined as

$$\dot{Q}_{max} = C_{min}(T_{h,i} - T_{c,i}), \tag{2.9}$$

where C_{min} is the smallest of C_c and C_h, which are the respective heat capacity rates for the cold and hot fluids. The heat capacity rate is calculated as

$$C = c_p\dot{m}, \tag{2.10}$$

where c_p is the specific isobaric heat capacity of the fluid. In GT-SUITE, the heat exchangers were parametrized geometrically, and also with tables correlating the input mass flow rate and temperatures to the actual heat transfer rate, provided by the manufacturer of the heat exchanger. By using the above mentioned equations, together with data on the specific heat capacity of the media from TILMedia Suite [13], a table correlating the mass flow rates of the primary and secondary sides of the heat exchanger to the effectiveness could be computed. This is the required input data for a heat exchanger of type StaticEffiencyTable in LCL.

For any heat exchanger, it is true that [8]

$$\varepsilon = f\left(\text{NTU}, \frac{C_{min}}{C_{max}}\right), \tag{2.11}$$

where C_{min}/C_{max} is equal to either C_c/C_h or C_h/C_c depending of the relative magnitudes, and is referred to as C_r. f is a function which depends on the flow arrangement of the heat exchangers. The number of transfer units (NTU) is a dimensionless parameter defined as

$$\text{NTU} \equiv \frac{UA}{C_{min}} \tag{2.12}$$

where UA is the overall heat transfer coefficient. These epsilon functions depend on the type of heat exchanger used and the ones relevant are presented in Table 2.2. The mentioned functions are provided in LCL, with the exception of Crossflow with both fluids unmixed.

Table 2.2: Heat Exchanger Effectiveness Relations [8]

Flow Arrangement	Relation
Counterflow	$\varepsilon = \frac{1-\exp[-\mathrm{NTU}(1-C_r)]}{1-C_r\exp[-\mathrm{NTU}(1-C_r)]}, (C_r < 1)$
	$\varepsilon = \frac{\mathrm{NTU}}{1+\mathrm{NTU}}, \quad (C_r = 1)$
Crossflow	
Both fluids unmixed	$\varepsilon = 1-\exp\left[\left(\frac{1}{C_r}\right)(\mathrm{NTU})^{0.22}\{\exp[-C_r(\mathrm{NTU})^{0.78}]-1\}\right]$
C_{max} (mixed), C_{min} (unmixed)	$\varepsilon = \left(\frac{1}{C_r}\right)(1-\exp\{-C_r[1-\exp(-\mathrm{NTU})]\})$
C_{min} (mixed), C_{max} (unmixed)	$\varepsilon = 1-\exp(-C_r^{-1}\{1-\exp[-C_r(\mathrm{NTU})]\})$

The overall heat transfer coefficient may be expressed as

$$\frac{1}{UA} = \frac{1}{h_c A_c} + \frac{t_w}{k_w A_w} + \frac{1}{h_h A_h} \tag{2.13}$$

where $h_{c,h}$ are heat transfer coefficients for the cold and hot fluids, A_c the heat transfer area for the cold fluid, A_w the heat transfer area for the wall, and A_h the heat transfer area for the hot fluid. t_w and k_w are the thickness of the wall, and thermal conductivity, respectively. In LCL the relation is simplified as

$$\frac{1}{UA} = \left(\frac{1}{h_c} + \frac{t_w}{k_w} + \frac{1}{h_h}\right)\frac{1}{A_{heat}} \tag{2.14}$$

as such, the model is only geometrically valid when $A_w = A_h = A_c$. However, the heat transfer coefficients in Dymola may be corrected with calibration factors CF_c, CF_h. By setting $A_{heat} = A_w$, $CF_c = \frac{A_c}{A_w}$ and $CF_h = \frac{A_h}{A_w}$ we arrive at the original equation 2.13. The relevant epsilon function, together with the wall properties and calibration factors, are necessary input values for a heat exchanger model of type EpsNTU in LCL.

2.4 Approximation of boundary conditions

In the Dymola models, a very important part is to properly assign the boundary conditions. For the most part, these quantities had been measured and were deemed to be accurate. However, the properties that were hardest to quantify were those of the cooling headwind. A lack of sensors meant that neither the pressure nor the mass flow rate were measured, and approximations were needed.

In GT-SUITE, the total cooling air pressure due to ambient pressure and head wind velocity is defined as of Bernouilli's principle.

$$p_{total} = p_{static} + \frac{1}{2} c_{pc} \rho v^2 \tag{2.15}$$

where c_{pc} is the head wind pressure coefficient, which for flow entering a system is $c_{pc} \in [0,1]$ and for flow exiting a system, $c_{pc} \in [-1,0]$. [7]

With these approximations, together with pressure drop models for the heat exchangers, pressure increase by the fan, and general pressure loss due to friction in the engine room, Dymola computed a mass flow rate of the air. This curve was then approximated as a function of vehicle speed, fan speed, and their respective squares.

It was found that only having pressure boundaries for the air flow caused numerical instability, especially when using fix-step solvers, and as such it was important to approximate the mass flow rate function to use as a boundary condition.

3

Implementation of the Model

3.1 Validation

The model validation was done by comparing the simulation results to the actual measured data. In the thermodynamical sense, the aim was to minimize the error in simulated temperature and heat transfer rates. For fluid dynamics, focus was on getting the pressure and mass flow rate correct.

3.2 Model calibrations and optimization

Some of the model parameters were not retrievable from GT-SUITE, and as such had to be estimated in the Dymola model. Examples of this are the calibration factors for heat transfer or pressure loss in the heat exchangers, or other unknown pressure drops in the cycle. To get approximate and acceptable values for these parameters, some kind of model optimization had to be used.

Most of the model optimization was done in MATLAB using the global optimization toolbox from Mathworks and the FMI-toolbox from Modelon. By sweeping parameters, e.g. a pressure loss coefficient, the root mean square of the error between the measured and the simulated values could be computed. This RMSE was then used as the cost function which the algorithm was set to minimize. However, each function call of the optimization algorithm is one simulation of the model, which, depending on its size, takes up to a few minutes to complete.

As the minimization targets often did not have any explicit derivative functions, using an optimization algorithm which did not depend on gradients was preferred. For this reason, the algorithm pattern search was selected. This algorithm is derivative free and uses function calls with modesty. It also has proven global convergence, and

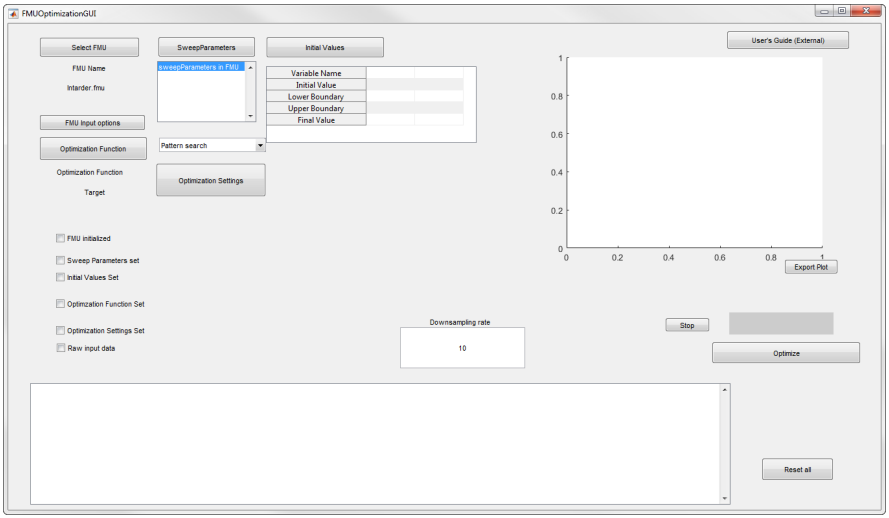

Figure 3.1: Optimization GUI main window.

is recommended by MathWorks to use when looking for a single global minimum [6]. A GUI which combined the features of the two toolboxes was developed, and is shown in Figure 3.1. This GUI gave a more general overview of the optimization process and parameter settings.

The parameters which were optimized were mainly lumped friction coefficients, replacing multiple pressure drop components. Examples of this are the pressure drop occurring in the engine, and the retarder. Calibration coefficients present in the LCL models of the heat exchangers, for pressure drop and heat transfer, were also optimized.

3.3 Solver options

Dymola includes a wide selection of integration algorithms, both variable step and fix step solvers. In line with MAN's earlier use of Dymola, CVODE was used for variable step simulation in the modeling process. Further on in the process, the Euler algorithms, implicit and explicit,were used and evaluated for use on the real time system.

In order for the real time simulation to be sufficiently fast, the step size of the fix step integrators must be as large as possible while retaining the properties and dynamics of the original model. As the sample time of the equipment in the engine was 0.05 seconds, this step size was the target. Another important aspect is that the simulation computational time per time step does not differ much between time steps. This is

to make sure that there is no bottleneck in the model which may cause severe delays in the real time simulation.

3.4 HIL implementation

A model which contained a table which output the boundary conditions of 71 steady state points, as well as customizable input values, and the cooling cycle was exported to Simulink from Dymola, with its inline integration method. In Simulink it was created with a Dymola block [3], compiled and built to a dSpace compatible file. However, a missing library file caused a problem. The heat exchangers which were parametrized with a static efficiency table were not exportable, and as such they had to be replaced with Eps-NTU parametrization models.

A crude simulation test bench was created in the dSpace Control Desk environment to test if the model would run in real time. This test bench is shown in Figure 3.2. On the left hand side, the model step size, turnaround time, overrun count, and the current state is shown. The slider bar at the bottom controls which state is being simulated. The two plot graphs show the simulated (green) and measured value (red) of the mass flow rate (left) and pressure (right) of the coolant in the high pressure charge air cooler.

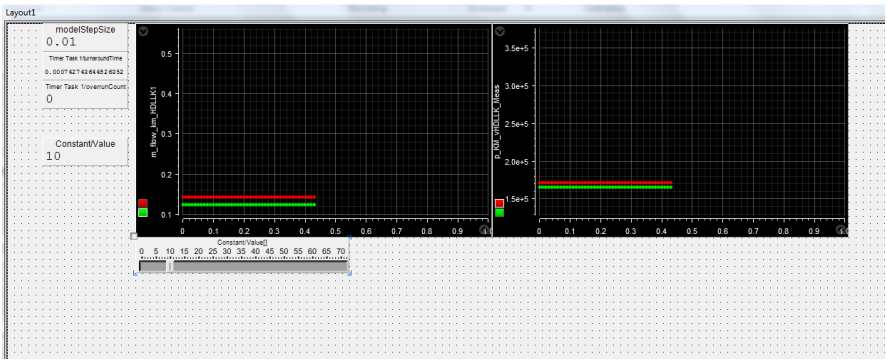

Figure 3.2: dSpace Control Desk test bench GUI.

4

Results

4.1 Component test benches

The component test benches generally gave acceptable results, as the boundary conditions were clearly defined and no flow branching modeling was needed. In the following pages, plots of these results are presented for the high and low pressure charge air coolers, which were focus points at the early stages of the thesis. On the upper left hand side, the transient cycle simulation results are displayed.

On the upper right hand side, the simulated values are in a scatter plot versus the measurement values, together with confidence intervals of $\pm 10\%$. The simulated values are obtained from the steady state simulations. The lower right hand side graph shows the error value in the transient cycle. In all cases except temperature, it shows the relative error, calculated as $\eta_{rel} = \eta_{abs}/v_{meas}$, where $\eta_{abs} = v_{sim} - v_{meas}$, v_{sim} and v_{meas} are the simulated and measured values, respectively. For temperature it shows the absolute error in K.

For the thermodynamic part, the results shown are temperature and heat flow rate. For the fluid dynamic part, the results shown are pressure and/or mass flow rate.

4.1.1 Low pressure charge air cooler

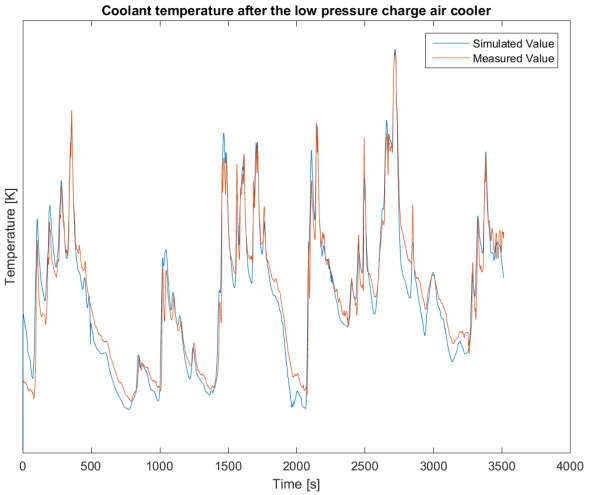

Figure 4.1: Simulation values and measured values of the coolant temperature after the low pressure charge air cooler in the transient cycle.

This is a cooler parametrized as an efficiency table heat exchanger. As shown in Figure 4.1, the temperature of the coolant generally follows the measured values, with the exception of at peaks and valleys. This can be due to the fact that the thermal intertia of the heat exchanger solid mass is not properly included. In the steady state case, shown in Figure 4.2, the scatter closely follows the measured value curve, with slight deviations at the lowest and highest temperature. In Figure 4.3 the absolute error is shown, and we can see that at most the simulation deviates about 8 K from the measurement, and at most points is the deviation is even lower.

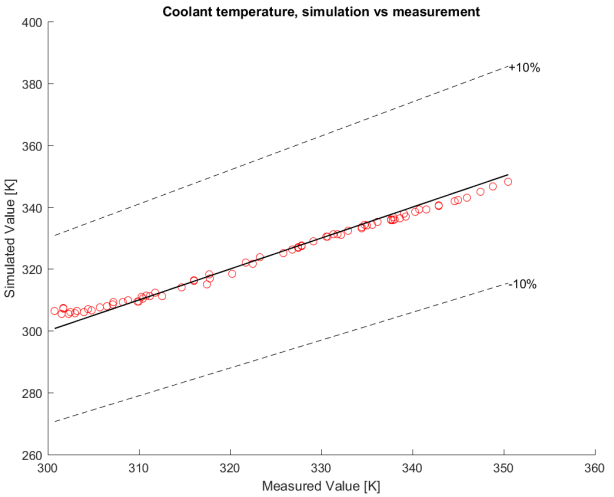

Figure 4.2: Simulation values vs measurement values of the coolant temperature after the low pressure charge air cooler in the steady state cases.

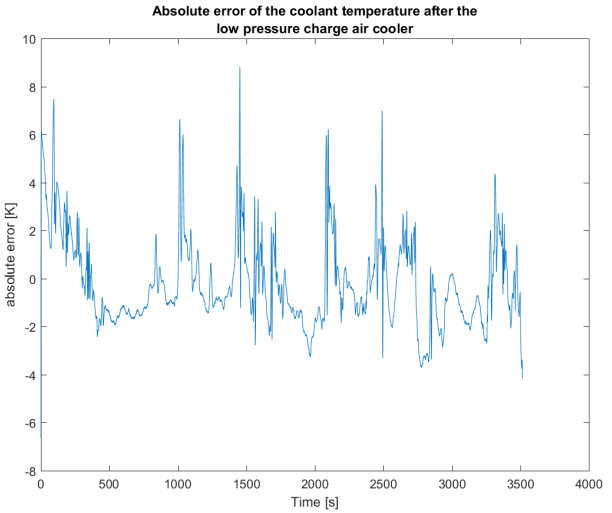

Figure 4.3: Absolute error of the coolant temperature after the low pressure charge air cooler in the transient cycle.

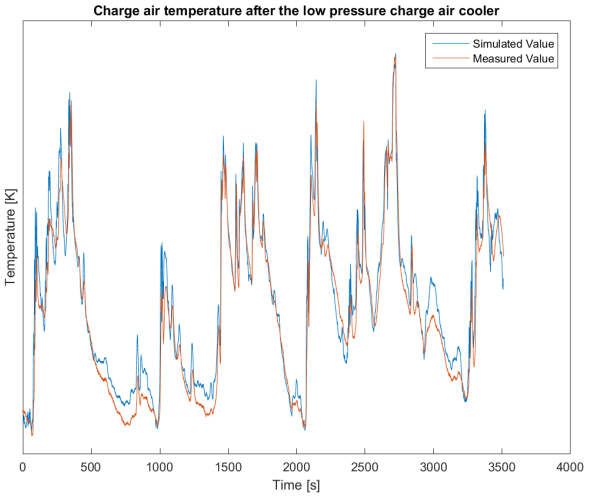

Figure 4.4: Simulation values and measured values of the charge air temperature after the low pressure charge air cooler in the transient cycle.

The charge air temperature, shown in Figures 4.4 & 4.5, is a bit high at times in the transient cycle simulation, but generally follows the curve in the steady state simulations. The transient cycle error is shown in Figure 4.6 and peaks at 10 K but is in general less than 2 K.

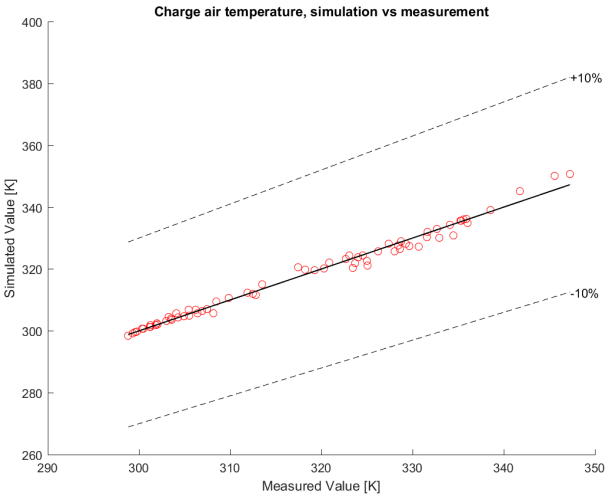

Figure 4.5: Simulation values vs measurement values of the charge air temperature after the low pressure charge air cooler in the steady state cases.

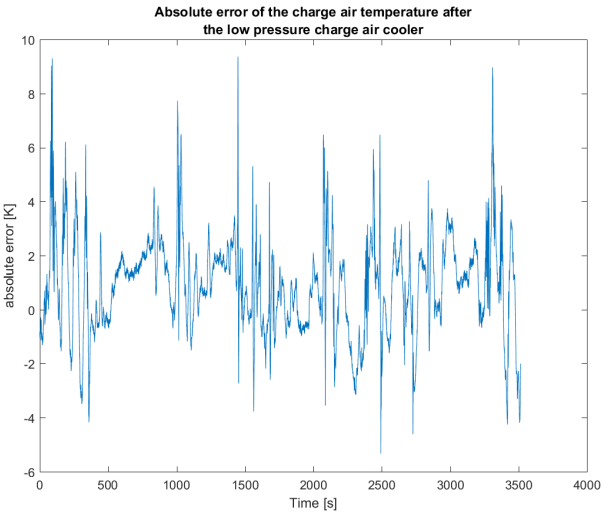

Figure 4.6: Absolute error of the charge air temperature after the low pressure charge air cooler in the transient cycle.

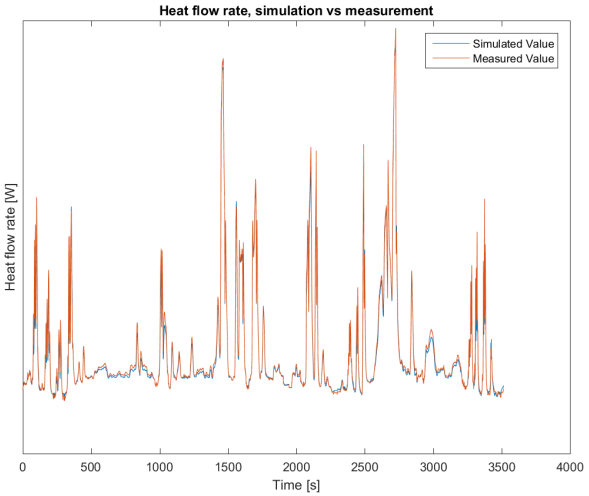

Figure 4.7: Simulation values and measured values of the heat flow rate in the low pressure charge air cooler in the transient cycle.

In Figures 4.7 & 4.8, the heat flow rate from the charge air to the coolant is displayed. Both of the figures display simulation values very close to the actual values, with very small deviations in some steady state cases. The heat flow relative error is shown in Figure 4.9. It is generally small in magnitude. However, it has several large spikes. Although it looks bad, it is probably due to the fact that the actual heat flow rate is so small that the relative error is exagerrated.

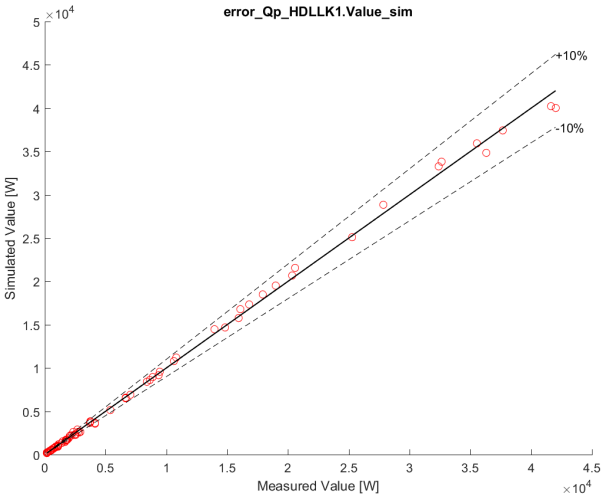

Figure 4.8: Simulation values vs measurement values of the heat flow rate in the low pressure charge air cooler in the steady state cases.

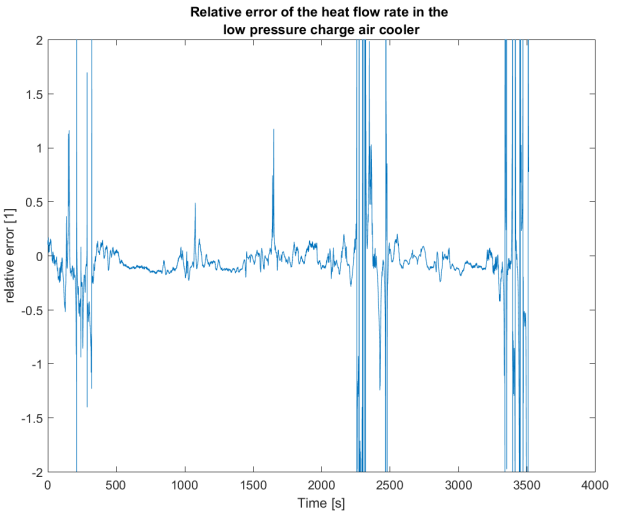

Figure 4.9: Relative error of the heat flow rate in the low pressure charge air cooler in the transient cycle.

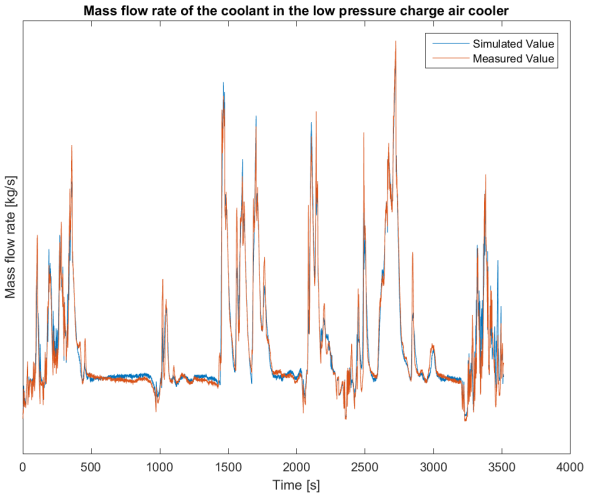

Figure 4.10: Simulation values and measured values of the coolant mass flow rate through the low pressure charge air cooler in the transient cycle.

For the fluid dynamics, the test bench was modeled with two pressure boundaries for the coolant side, leaving mass flow rate as a simulation result. For the transient cycle, it is shown in Figure 4.10, and it matches quite well. In the steady state cases, shown in Figure 4.11, it is displayed that for lower mass flow rates the deviation is larger. The mass flow rate relative error is displayed in Figure 4.12. The magnitude of the error is generally below 10 %.

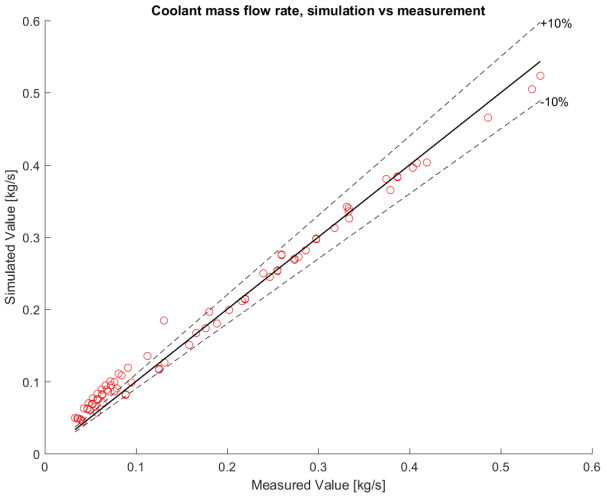

Figure 4.11: Simulation values vs measurement values of the coolant mass flow rate through the low pressure charge air cooler in the steady state cases.

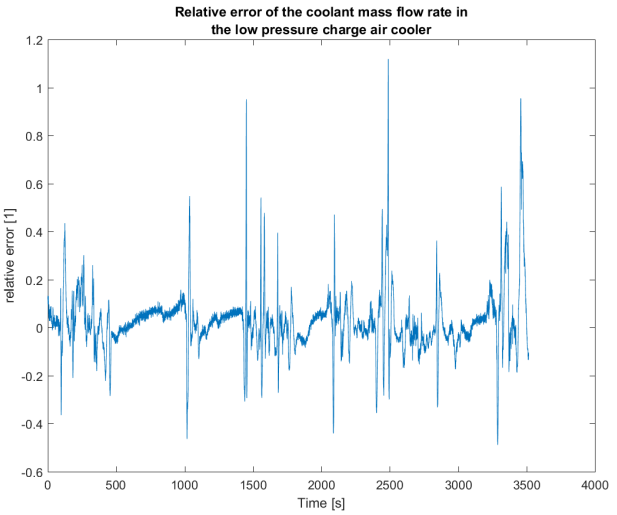

Figure 4.12: Relative error of the coolant mass flow rate in the low pressure charge air cooler in the transient cycle.

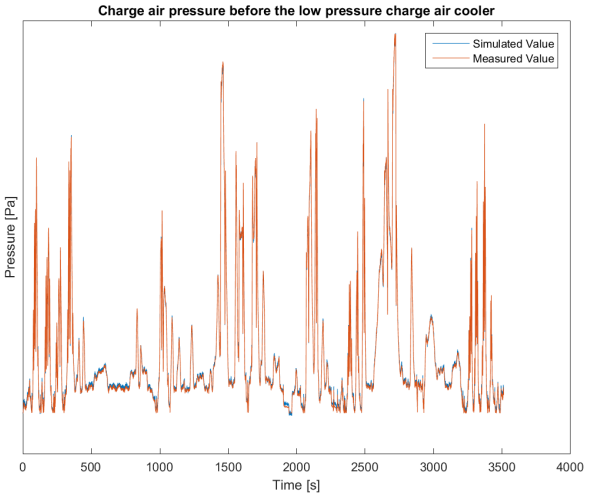

Figure 4.13: Simulation values and measured values of the charge air pressure before the low pressure charge air cooler in the transient cycle.

On the charge air side, one mass flow boundary and one pressure boundary was used, leaving the pressure before the cooler to be simulated. As shown in Figures 4.13 & 4.14, it is generally well modeled. This is further reinforced by Figure 4.15, which shows that the relative error lies below 3 % at all times.

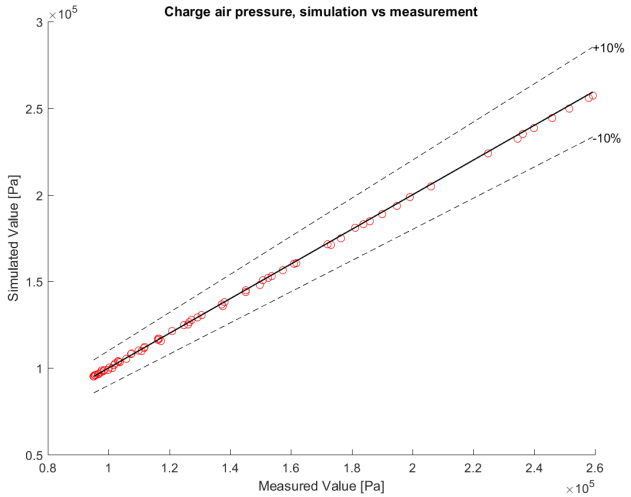

Figure 4.14: Simulation values vs measurement values of the charge air pressure before the low pressure charge air cooler in the steady state cases.

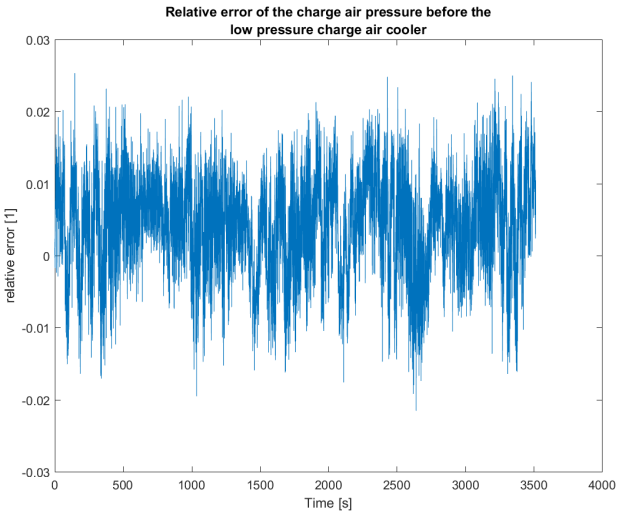

Figure 4.15: Relative error of the coolant mass flow rate in the low pressure charge air cooler in the transient cycle.

4.1.2 High pressure charge air cooler

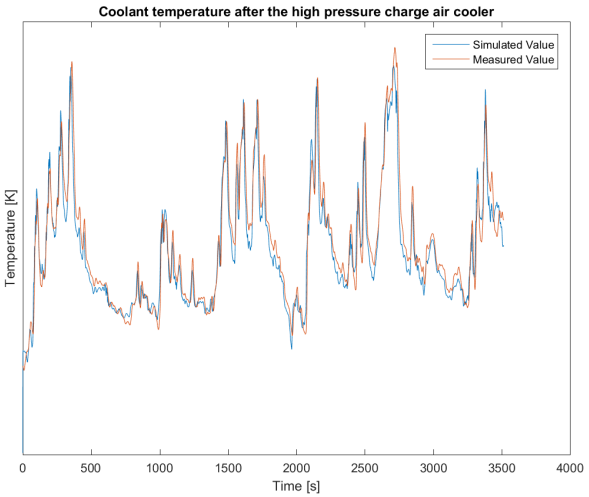

Figure 4.16: Simulation values and measured values of the coolant temperature after the high pressure charge air cooler in the transient cycle.

Just as the low pressure variant, the high pressure charge air cooler was parametrized in Dymola as an efficiency table heat exchanger. The transient temperature curve for the coolant, shown in Figure 4.16 follows the measurement, while the steady state scatter in Figure 4.17 hints at slight deviation at lower temperatures. The absolute error of the coolant temperature in Figure 4.18 shows that the magnitude of the error has its largest value at about 8 K, and is generally below 2 K.

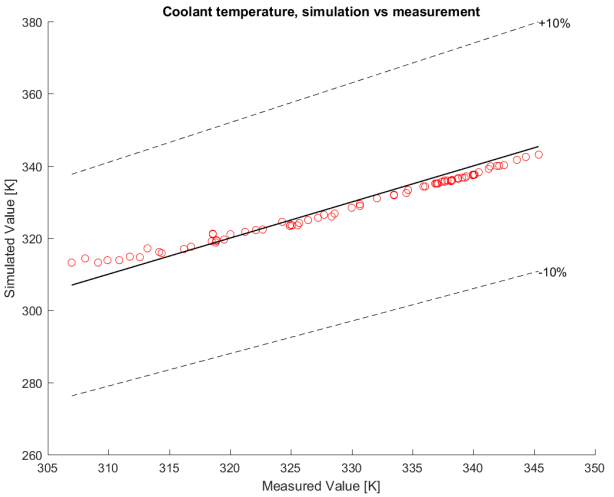

Figure 4.17: Simulation values vs measurement values of the coolant temperature after the high pressure charge air cooler in the steady state cases.

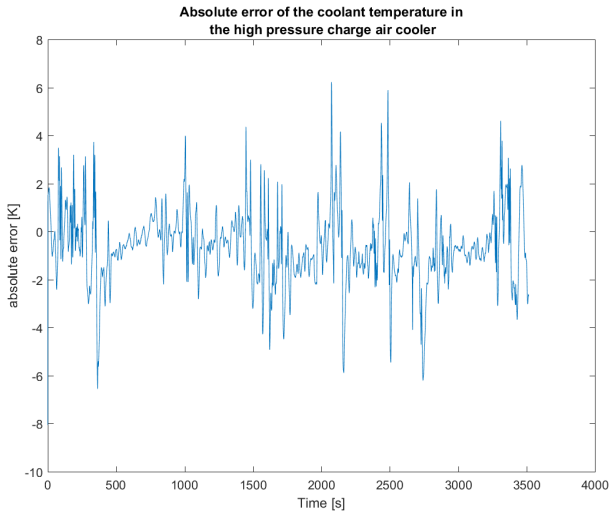

Figure 4.18: Absolute error of the coolant temperature after the high pressure charge air cooler in the transient cycle

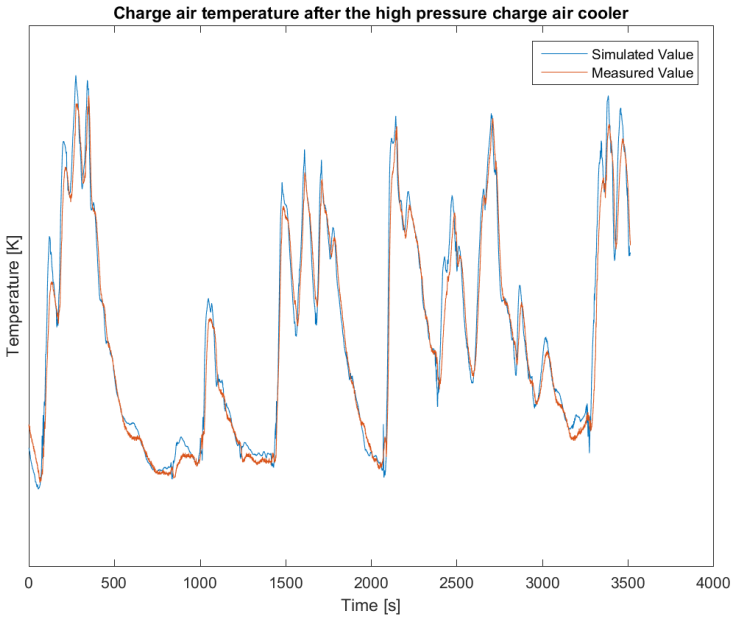

Figure 4.19: Simulation values and measured values of the charge air temperature after the high pressure charge air cooler in the transient cycle.

The charge air temperature after the high pressure cooler, displayed in Figures 4.19 & 4.20 closely corresponds to the measured values, with a few overshoots at the peaks. This is reflected in Figure 4.21, where the absolute error at the peaks is several degrees larger than at the lower temperatures.

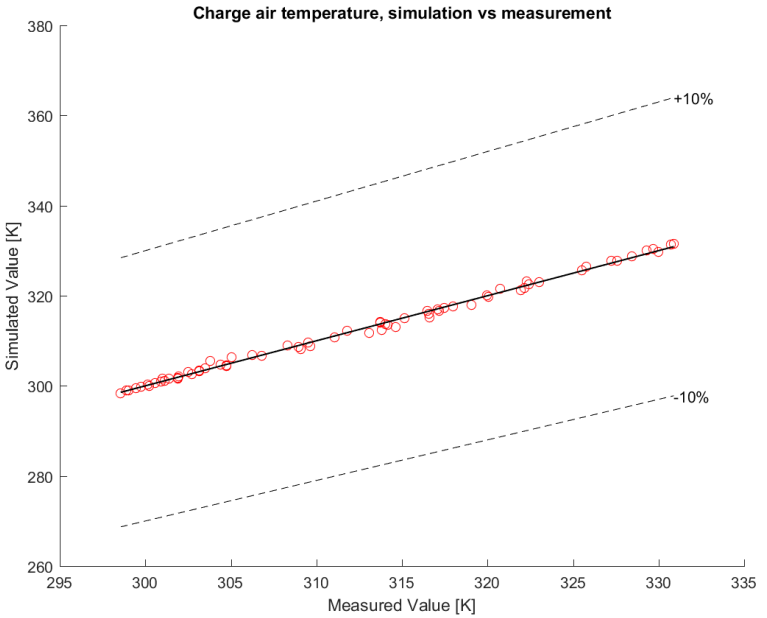

Figure 4.20: Simulation values vs measurement values of the charge air temperature after the high pressure charge air cooler in the steady state cases.

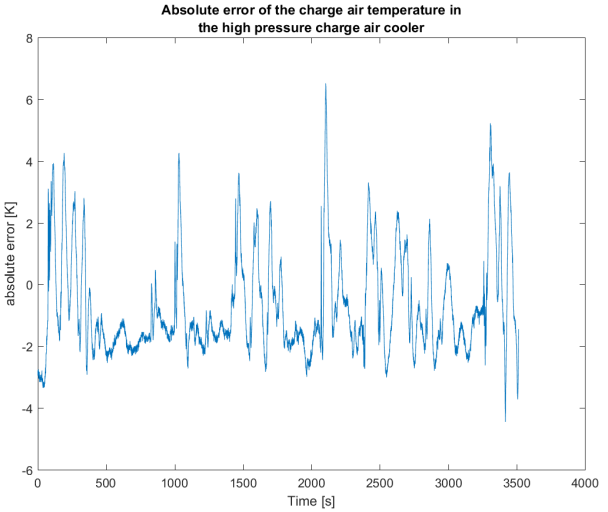

Figure 4.21: Absolute error of the charge air temperature after the high pressure charge air cooler in the transient cycle

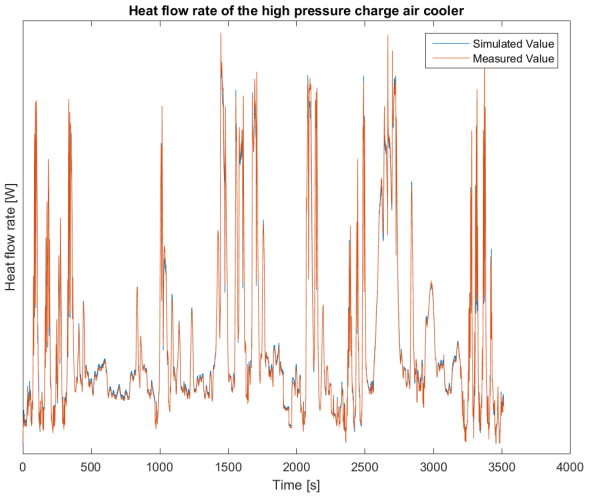

Figure 4.22: Simulation values and measured values of the heat flow rate in the high pressure charge air cooler in the transient cycle.

The heat flow rate, as shown in Figure 4.22, is almost indistinguishable from the measurement values, and Figure 4.23 confirms that this holds for all the steady state cases as well. Looking at the relative error in Figure 4.24, it is less than 5 % at almost all measurement points in the transient cycle.

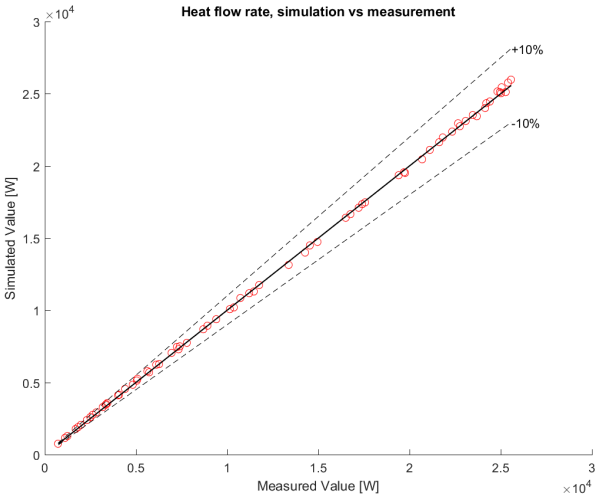

Figure 4.23: Simulation values vs measurement values of the heat flow rate in the high pressure charge air cooler in the steady state cases.

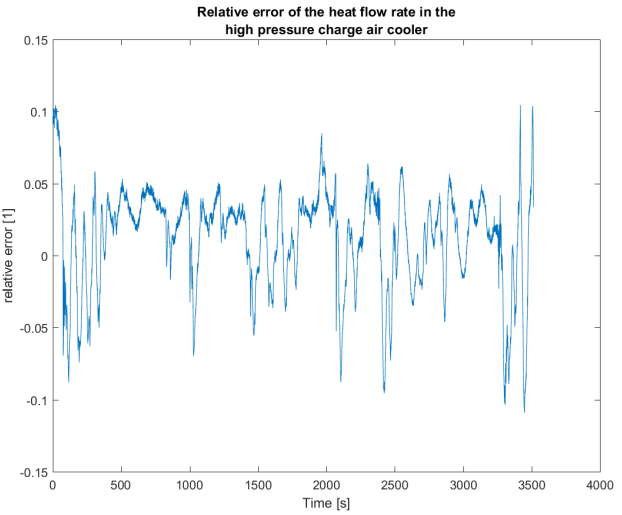

Figure 4.24: Relative error of the heat flow rate in the high pressure charge air cooler in the transient cycle.

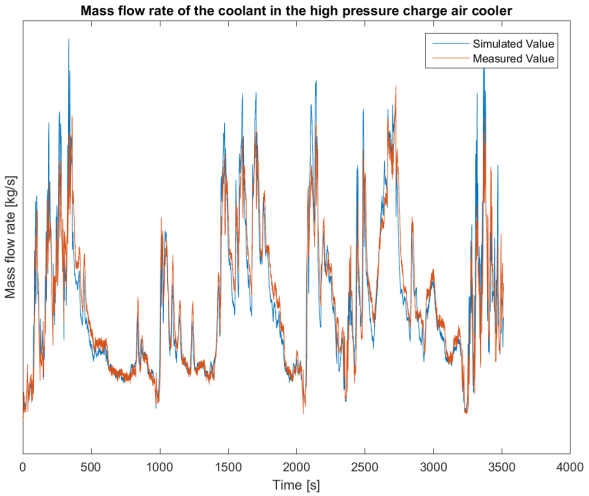

Figure 4.25: Simulation values and measured values of the coolant mass flow rate in the high pressure charge air cooler in the transient cycle.

For the pressure dynamics, Figures 4.25 & 4.26 displays a close result for the coolant mass flow rate. There are overshoots at the peaks, though. The relative error, as shown in Figure 4.27 generally lies within $\pm$ 20 %, at some short intervals however, it is as large as 120 %. These spikes are quite short in duration, and do not seem to affect the total accuracy of the system that much.

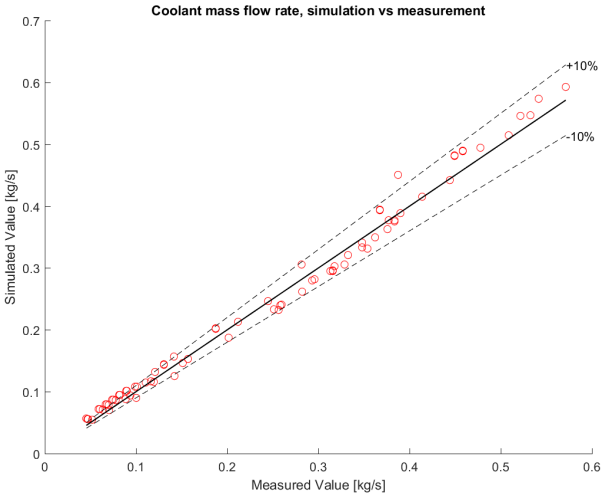

Figure 4.26: Simulation values vs measurement values of the coolant mass flow rate in the high pressure charge air cooler in the steady state cases.

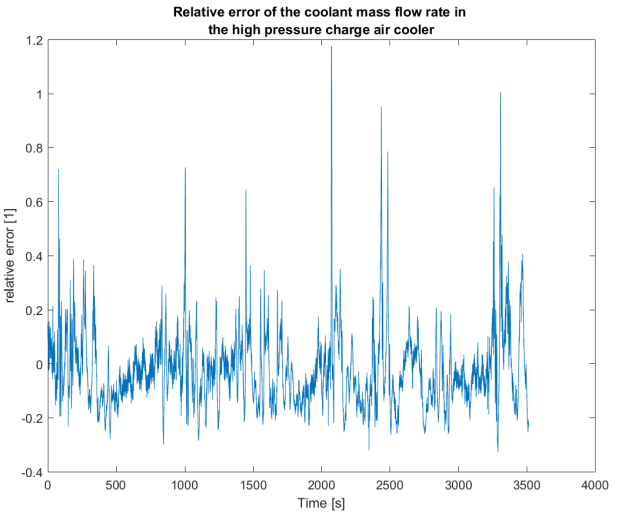

Figure 4.27: Relative error of the coolant mass flow rate in the high pressure charge air cooler in the transient cycle.

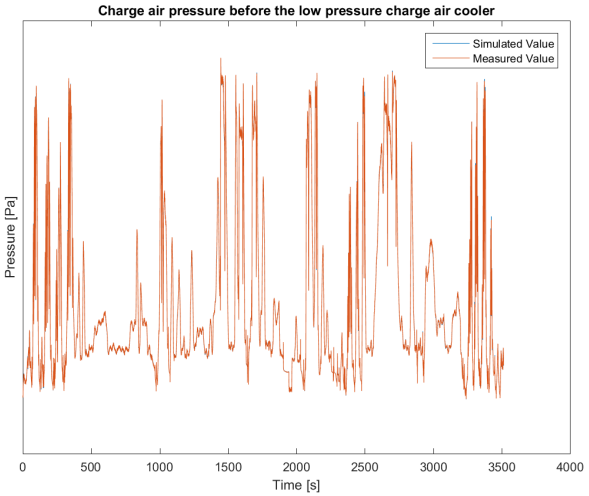

Figure 4.28: Simulation values and measured values of the charge air pressure before the high pressure charge air cooler in the transient cycle.

As for the charge air pressure before the high pressure charge air cooler, Figures 4.28 & 4.30 show that in the transient case, the relative error is less than 1 % most of the time. In the steady state cases shown in Figure 4.29, it is shown that every steady state simulation point matches well with the measurements.

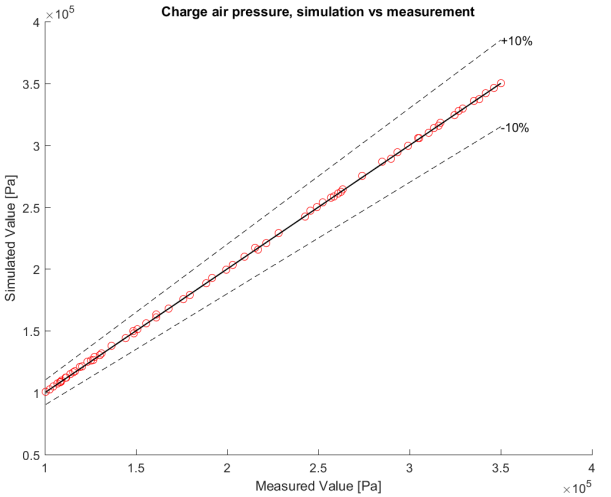

Figure 4.29: Simulation values vs measurement values of the charge air pressure before the high pressure charge air cooler in the steady state cases.

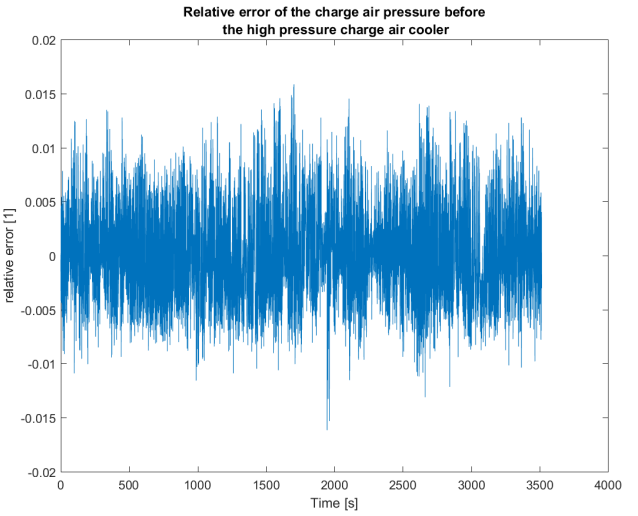

Figure 4.30: Relative error of the charge air pressure before the high pressure charge air cooler in the transient cycle.

4.1.3 Heat exchanger stack

The heat exchanger stack at the front of the vehicle consists of the low temperature cooler and the high temperature cooler. In the stack models provided by LCL, one of the boundary conditions for the cooling air is required to be the mass flow rate. However, since that data was not accessible, an alternative stack model had to be created. This also led to a increase in difficulty in validating the model.

In the following result graphs, the pressure boundaries for the cooling air are defined as in Equation 2.15. The flow path for the air included the two coolers, a pressure drop representing the radiator in front of the cooling package, the fan pressure increase and an extra calibrated pressure loss component. The test bench model used is shown in Figure 4.31, which aside from components included in the Liquid Cooling Library, contains a custom made stack model.

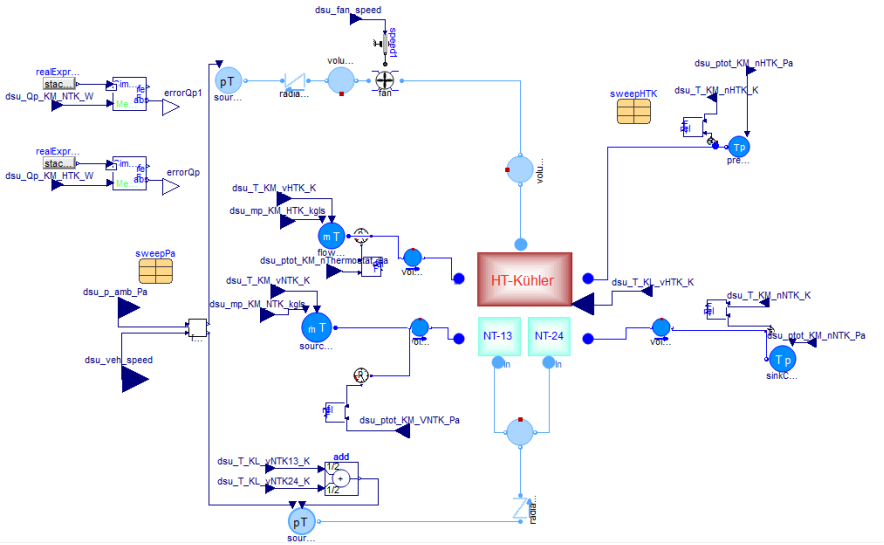

Figure 4.31: Pressure driven heat exchanger stack test bench.

In the custom heat exchanger stack model, shown in Figure 4.32, the low temperature cooler is discretized as two separate heat exchangers, where the coolant flow is serial, separated with a volume model connected to a wall, which is a model of heat capacity for solid material. The parameters for the heat transfer model were taken from the physical geometry of the wall. The air flow in the low temperature cooler(s) is parallel, and is joined before the high temperature cooler [1], which is modeled as a single cooler. Both the low and high temperature cooler were parameterized as Epsilon NTU coolers, as splitting the cooler yielded unsatisfactory results with the efficiency table parametrization.

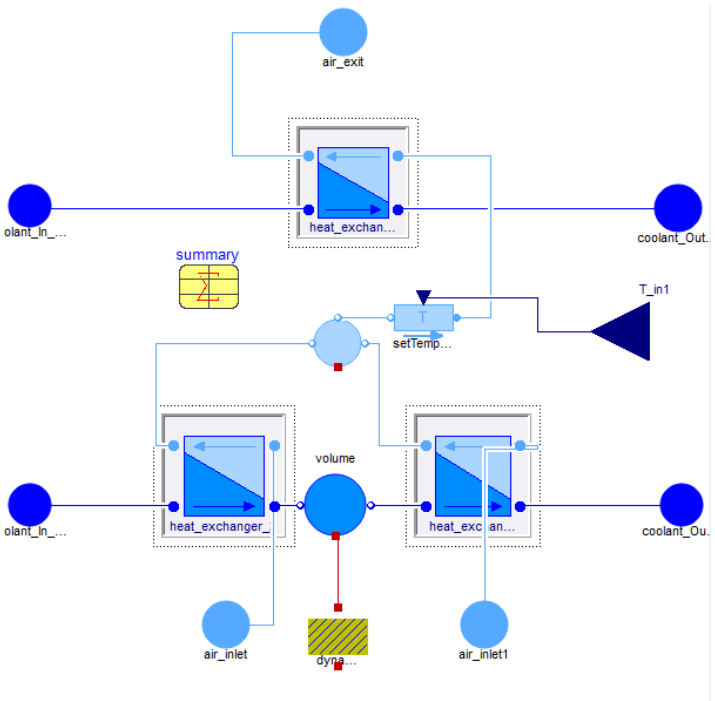

Figure 4.32: Heat exchanger stack model

[1] The imposed temperature on the air in between the coolers was used during modeling at not required in the final model.

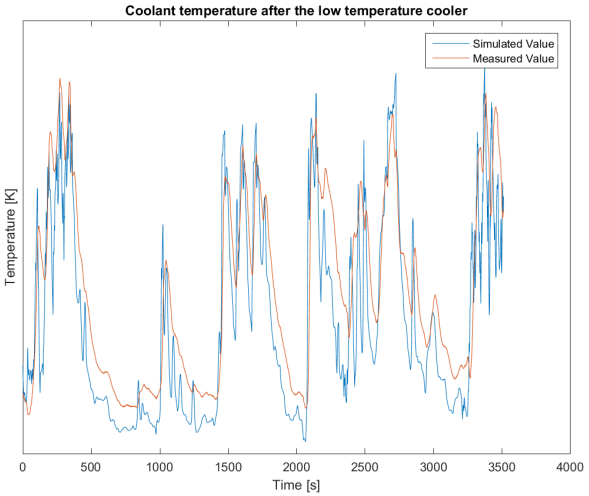

Figure 4.33: Simulation values and measured values of the coolant temperature after the low temperature cooler in the transient cycle.

In Figures 4.33 & 4.34 the coolant temperature after the low temperature cooler(s) is shown. It follows the general outline well enough but deviates at the local maxima and minima, possibly an effect of insufficient thermal inertia modeling. Figure 4.35 shows the absolute error in the transient cycle, and once again shows that the temperature is lower than the measured value at the lower temperatures.

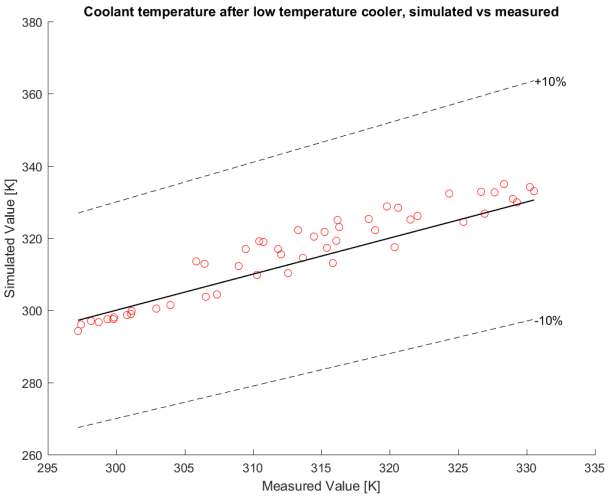

Figure 4.34: Simulation values vs measurement values of the coolant temperature after the low temperature cooler in the steady state cases.

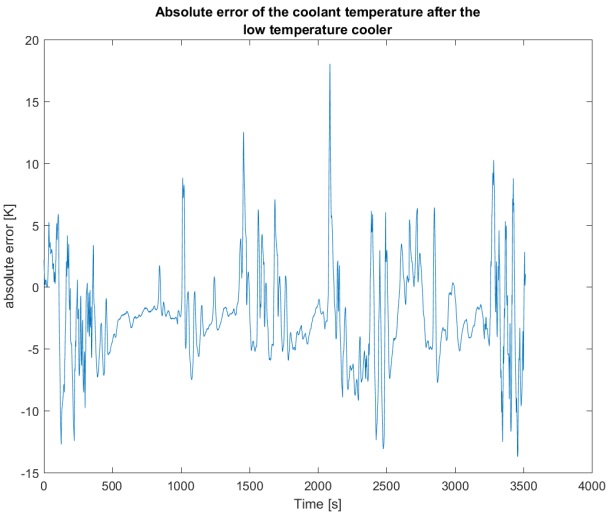

Figure 4.35: Absolute value of the error of the coolant temperature after the low temperature cooler in the transient cycle.

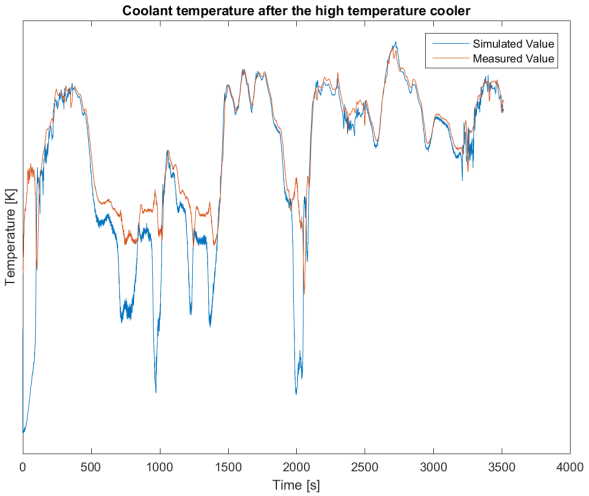

Figure 4.36: Simulation values and measured values of the coolant temperature after the high temperature cooler in the transient cycle.

For the high temperature cooler, in the transient case, shown in Figure 4.36, the curves coincide almost at all points, with the exception of the local minima, where the simulated value plummets further down than the actual measurement. This is mirrored in Figure 4.37, showing the steady state cases, where the simulated values lies closer to the measured values at higher temperatures than at lower. This is also shown in Figure 4.38, where the error magnitude is larger at the points at which the temperature is lower.

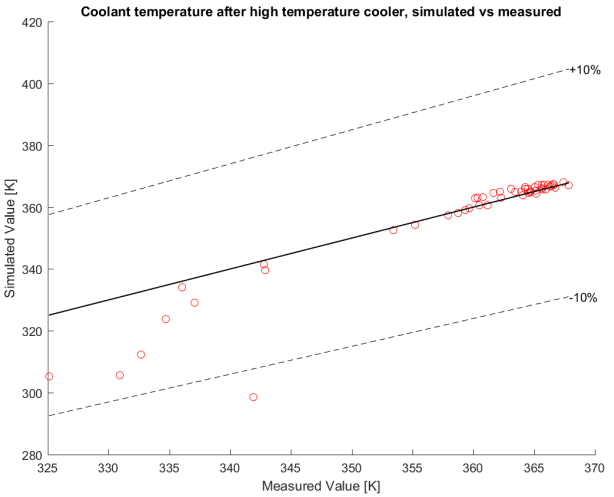

Figure 4.37: Simulation values vs measurement values of the coolant temperature after the high temperature cooler in the steady state cases.

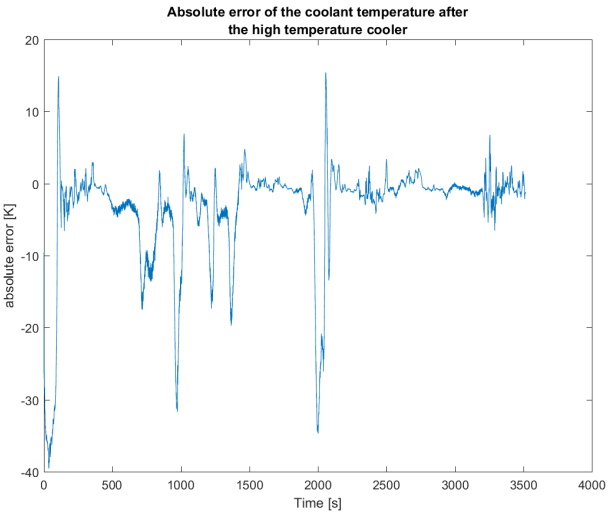

Figure 4.38: Absolute error of the coolant temperature after the high temperature cooler in the transient cycle.

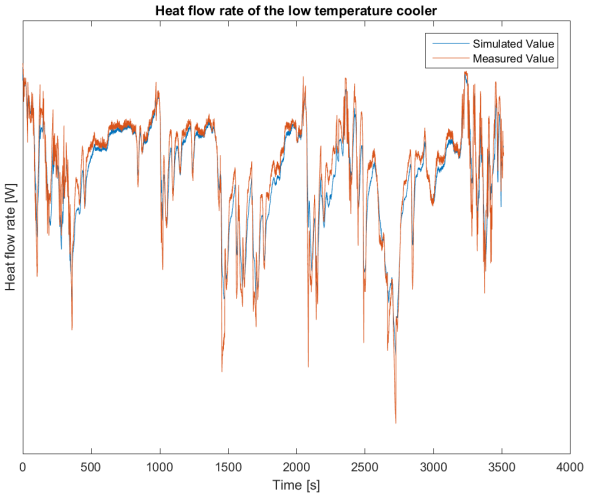

Figure 4.39: Simulation values and measured values of the heat flow rate in the low temperature cooler in the transient cycle.

Looking at the heat transfer rate, in Figure 4.39 we can see that in the transient case, the simulation values for the low temperature coooler are rather close to the measured values. The relative error is shown in Figure 4.41 and is generally smaller than 20 %. However, in the steady state cases displayed in Figure 4.40, we see that when the total magnitude of the heat transfer rate is larger, the simulation values are not large enough.

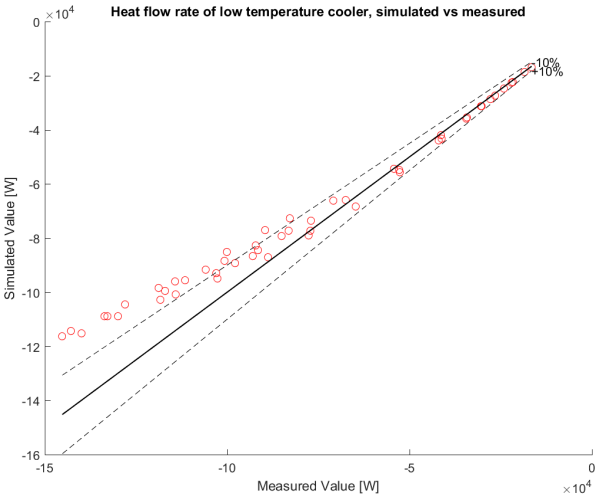

Figure 4.40: Simulation values vs measurement values of the heat flow rate in the low temperature cooler in the steady state cases.

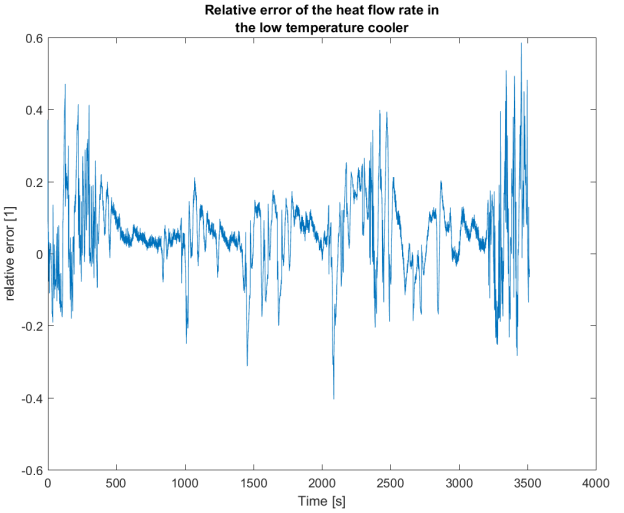

Figure 4.41: Relative error of the heat flow rate in the low temperature cooler in the transient cycle.

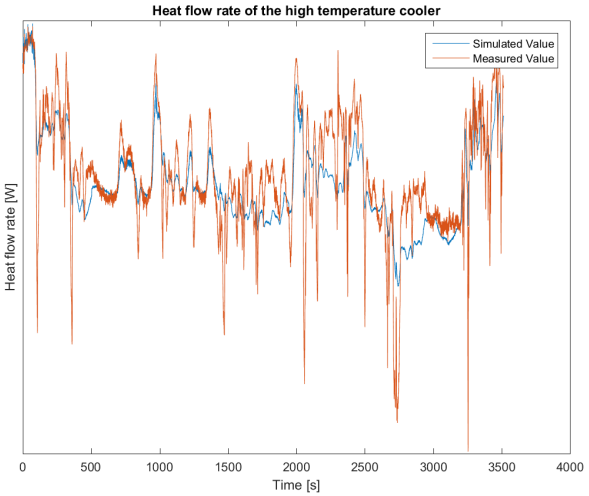

Figure 4.42: Simulation values and measured values of the heat flow rate in the high temperature cooler in the transient cycle.

The same applies to the high temperature cooler, where in the transient case, Figure 4.42, the value follows the curve, whereas in the steady state case, Figure 4.43, at the larger magnitudes of actual heat transfer rate, the simulation results deviate greatly. The relative error in the transient case is generally small, as shown in Figure 4.44, but at some points it is as large as 500 %, which is a very significant deviation.

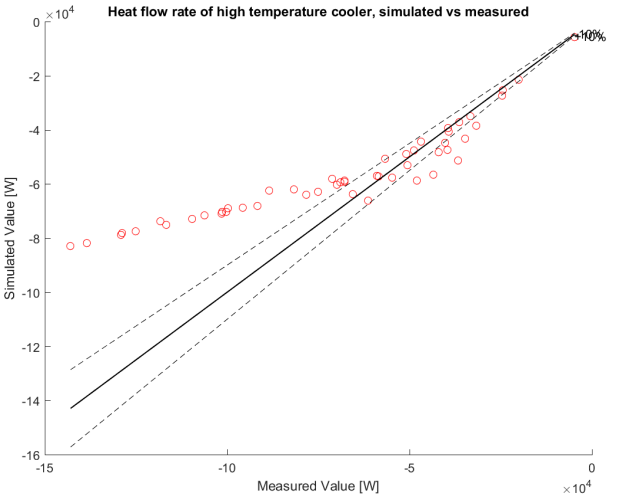

Figure 4.43: Simulation values vs measurement values of the heat flow rate in the low temperature cooler in the steady state cases.

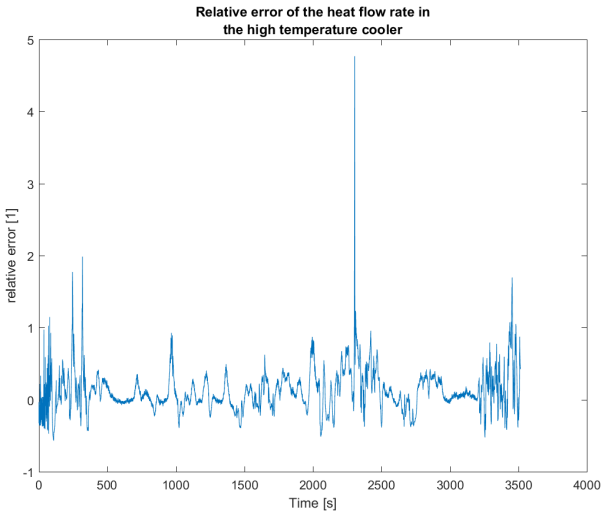

Figure 4.44: Relative error of the heat flow rate in the high temperature cooler in the transient cycle.

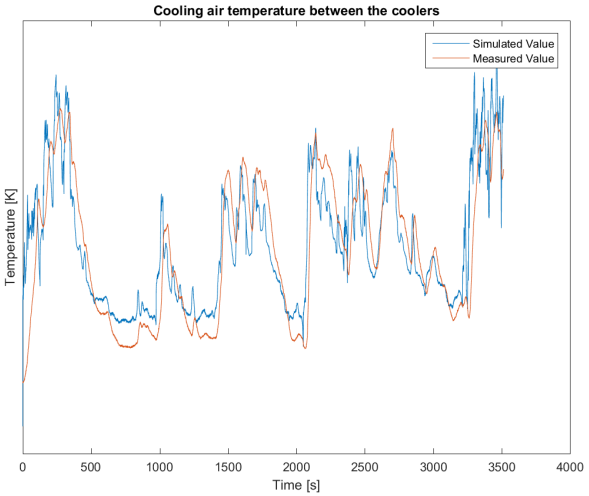

Figure 4.45: Simulation values and measured values of the cooling air temperature between the coolers in the stack in the transient cycle.

As for the cooling air temperatures between the coolers, Figures 4.45 and 4.46 show that the measured value is relatively close to the actual values on the entire spectrum. Figure 4.47, displaying the absolute error in K, shows that the sign of the error varies, but is generally smaller than 5 K.

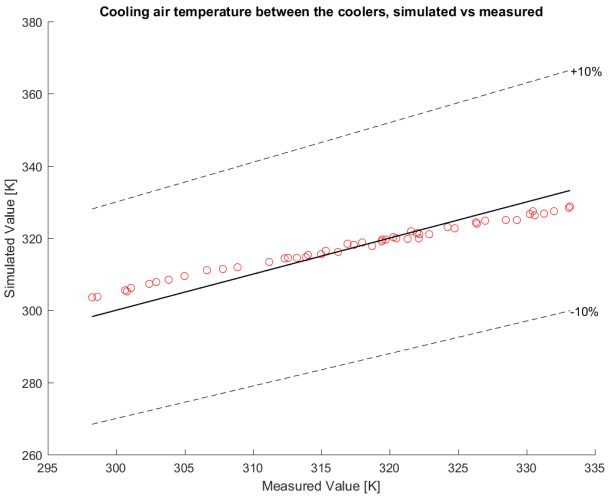

Figure 4.46: Simulation values vs measurement values of the cooling air temperature between the coolers in the stack in the steady state cases.

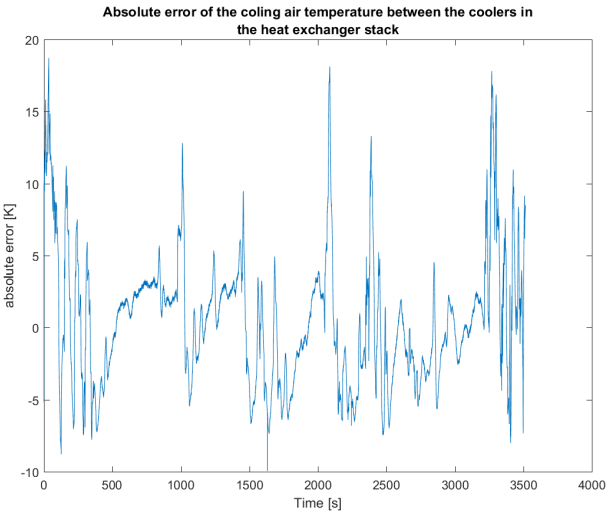

Figure 4.47: Absolute error of the cooling air temperature in between the coolers in the heat exchanger stack in the transient cycle.

4.2 Closed Circuit

Looking at the closed circuit model, an important validation point is getting the coolant mass flow rates correct. Since the medium model is incompressible, absolute pressure would not have a great impact on the flow rates. Rather, the pressure differences between the components governed the mass flow rate. As there was no measurement of the mass flow through the pump, it was hard to control whether the total mass flow of the system was correct or not. Most of the components, however, had measurements that could be assumed to be correct, and were used for validation.

In Figure 4.48, the branching components of the highest interest in the cycle are highlighted. From top to bottom, they are the split between the high pressure and low pressure charge air coolers, the split after the coolant pump dividing the low and high temperature cycle, and finally, the main thermostatic valve, which governs the flow to the high temperature cooler.

Starting at the coolant pump, the first branching mentioned occurs when most of the flow is directed to the crankshaft case and cylinder head, and part of the flow is directed to the low temperature cooler.

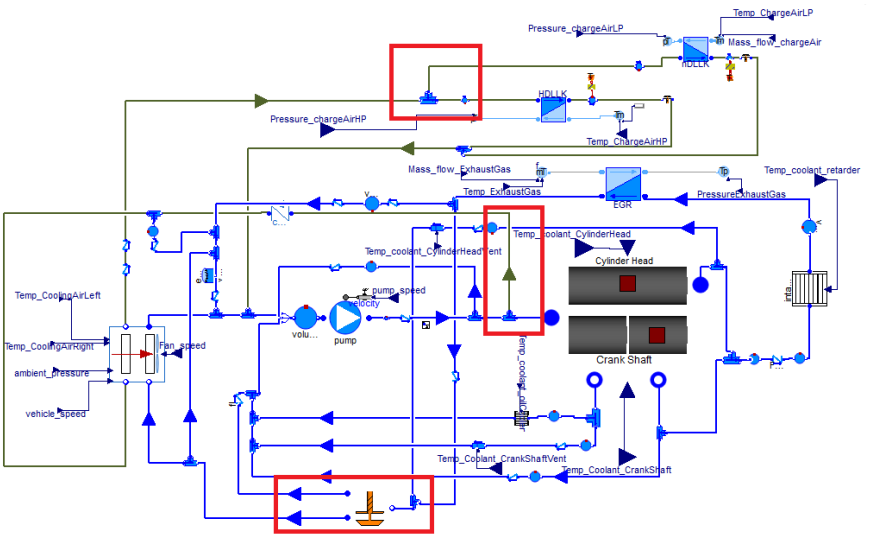

Figure 4.48: Cycle model highlighting the split components focsued on in this section.

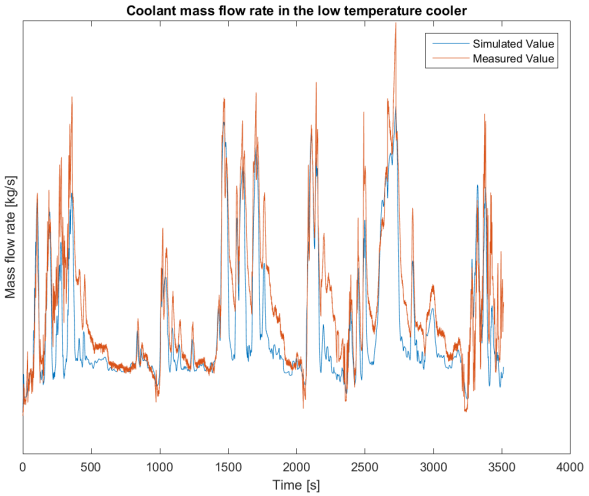

Figure 4.49: Simulation values and measured values of the coolant mass flow rate in the low temperature cooler in the transient cycle.

As presented in Figure 4.49 the simulation values of the coolant mass flow rate in the low temperature cooler followed the general outline of the measured ones, however, it was often too low, as is the most evident at the local minima. Figure 4.51 also shows that the relative error at times is close to 50 %, and at its highest it approaches 200 %. In the steady state cases, shown in Figure 4.50, the mass flow rates are generally within ± 10 % of the measured value, with a few scattered outliers.

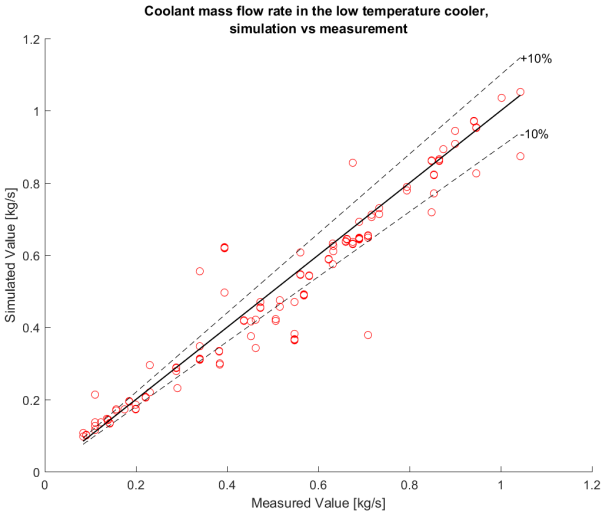

Figure 4.50: Simulation values vs measurement values of the coolant mass flow rate in the low temperature cooler in the steady state cases.

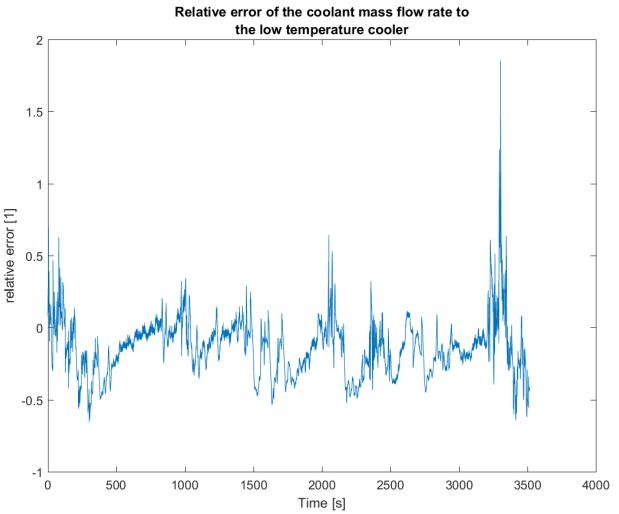

Figure 4.51: Relative error of the coolant mass flow rate in the low temperature cooler in the transient cycle.

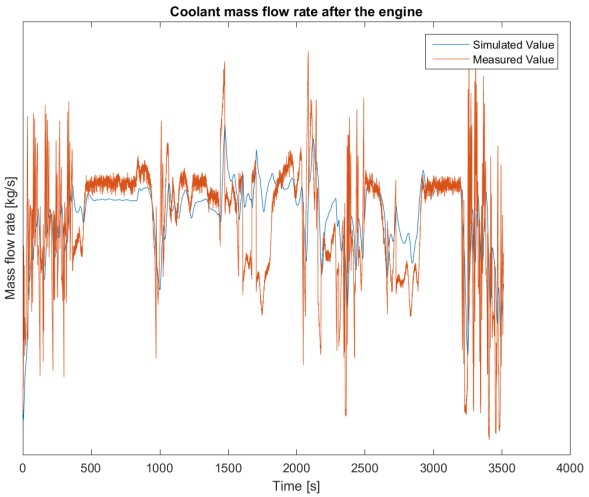

Figure 4.52: Simulation values and measured values of the coolant mass flow rate after the engine in the transient cycle.

As for the coolant flow through the engine components, the crankshaft case and the cylinder head, the results are for the transient cycle in Figure 4.52 and for the steady state cases in Figure 4.53. In the transient cycle, there are a few large deviations when the measured value decreases quickly and the simulation does not fully represent the changes. In the steady state case, the flow deviates at many points, though not greater than ten percent in most cases. The relative error in the transient cycle is displayed in Figure 4.54 and is generally small, with the exceptions of the deviations at around 1500 s and around 2500 s, as well as the parts in the beginning and the end of the cycle where the value is varying quickly.

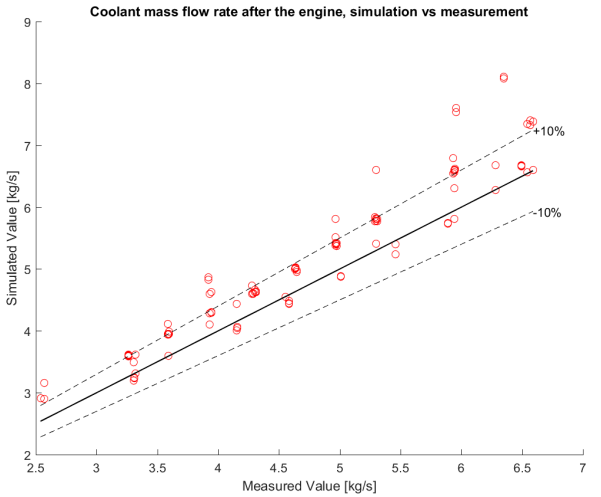

Figure 4.53: Simulation values vs measurement values of the coolant mass flow rate after the engine in the steady state cases.

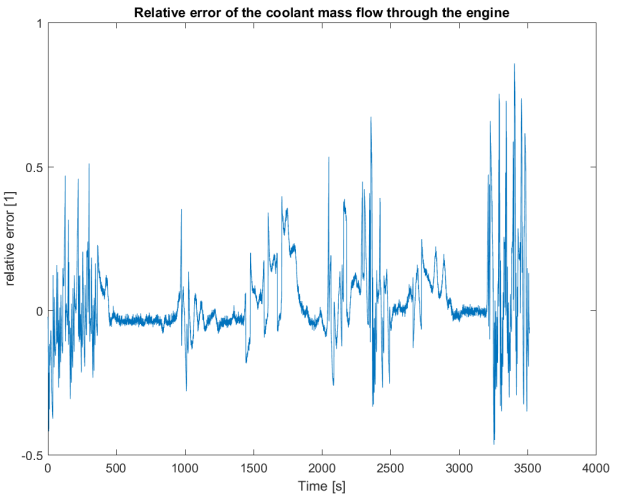

Figure 4.54: Relative error of the coolant mass flow rate through the engine in the transient cycle.

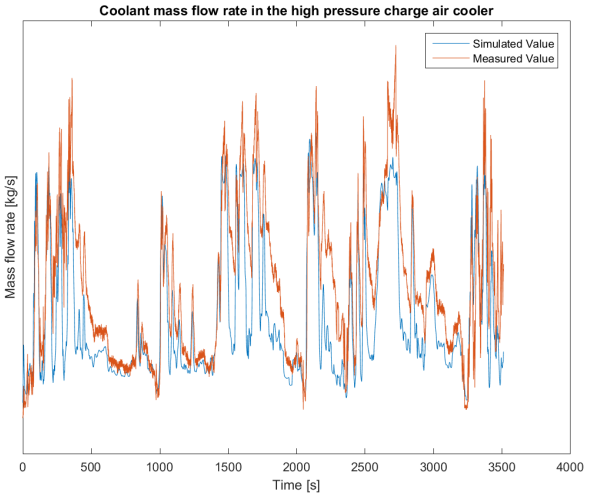

Figure 4.55: Simulation values and measured values of the coolant mass flow rate in the high pressure charge air cooler in the transient cycle.

Following the low temperature cycle, the next significant branching is after the low temperature cooler, where the flow branches to the high and low pressure charge air coolers, respectively. In Figures 4.55 & 4.56 the results for the high pressure charge air cooler are displayed. As can be seen in both the transient and steady state cases, the simulated flow rate is almost always lower than the actual flow. This can, however, be attributed to the lower flow rate in the low temperature cycle to begin with. This notion is reinforced by the fact that the relative error, shown in Figure 4.57 is strikingly similar of that for the low temperature cooler, recall Figure 4.51.

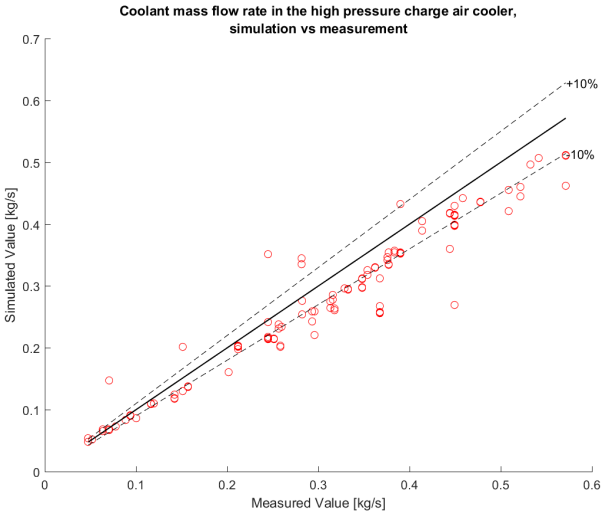

Figure 4.56: Simulation values vs measurement values of the coolant mass flow rate in the high pressure charge air cooler in the steady state cases.

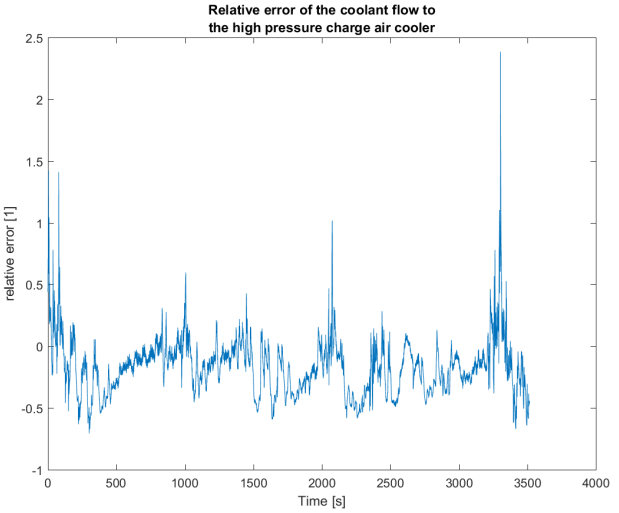

Figure 4.57: Relative error of the coolant mass flow rate through the high pressure charge air cooler in the transient cycle.

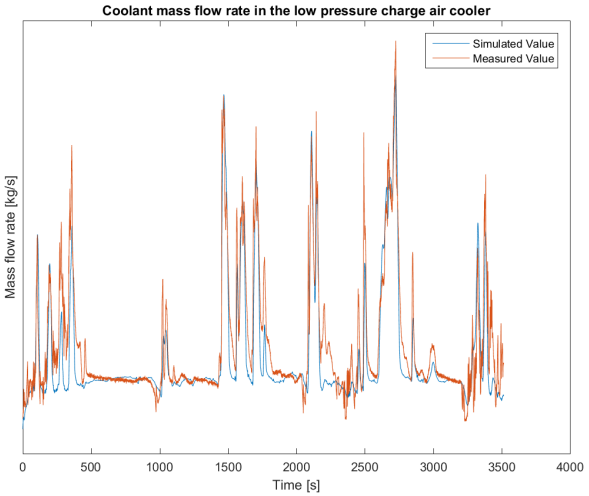

Figure 4.58: Simulation values and measured values of the coolant mass flow rate in the low pressure charge air cooler in the transient cycle.

For the low pressure charge air cooler, the coolant mass flow rate simulated value lies closer to the actual values than for the high pressure ditto. In Figure 4.58 the transient cycle simulation results are shown, and the simulation value are very reminiscent of the ones obtained in the test bench for the component, Figure 4.10. The steady state cases yield similar results, shown in Figure 4.59. The relative error in the transient case is shown in Figure 4.60, it as well shows that the simulated value is around 50 % smaller than the measured value, especially at the very dynamic sections.

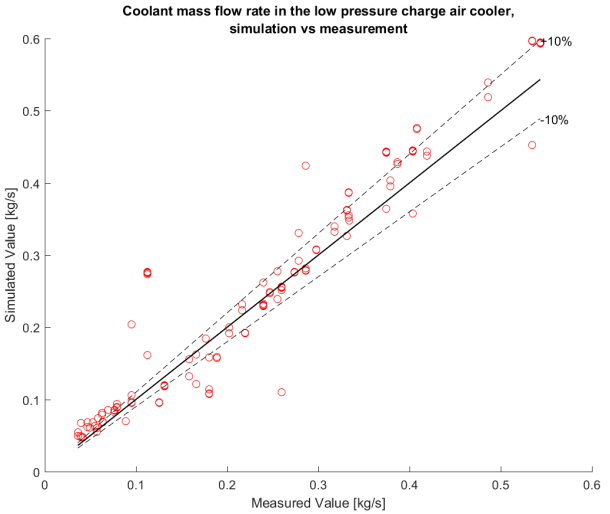

Figure 4.59: Simulation values vs measurement values of the coolant mass flow rate in the low pressure charge air cooler in the steady state cases.

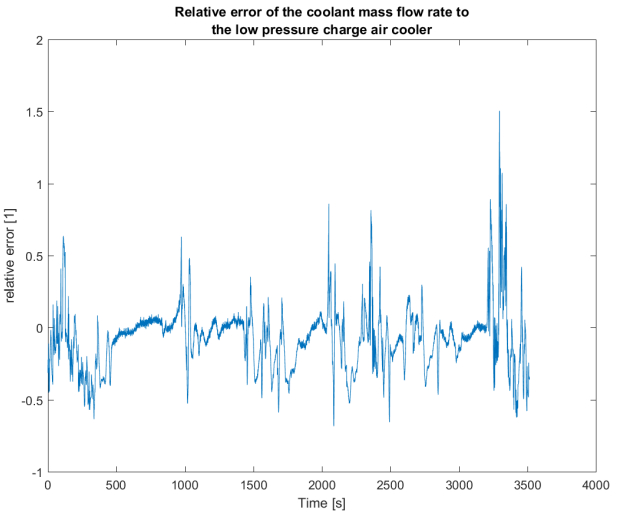

Figure 4.60: Relative error of the coolant mass flow rate through the low pressure charge air cooler in the transient cycle.

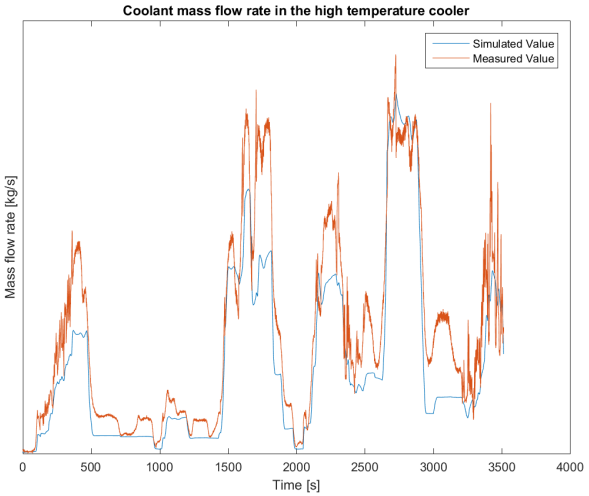

Figure 4.61: Simulation values and measured values of the coolant mass flow rate in the high temperature cooler in the transient cycle.

At the thermostat, the high temperature circuit is split between the main and the bypass valve. The main valve leads to the high temperature cooler. Unfortunately there was no data for the flow through the thermostatic bypass valve, and validation had to be done with only the main flow. As seen in Figure 4.61, in the transient cycle the mass flow rate deviates at most at the peaks, not reaching high enough. This is further shown in Figure 4.63, where the relative error is shown. The relative error lies between $-100\,\%$and $0\,\%$, once again displaying quite poor performance. However, in the steady state cases, shown in Figure 4.62, with a few exceptions, the simulation values lies within a $10\,\%$ range of the measured values.

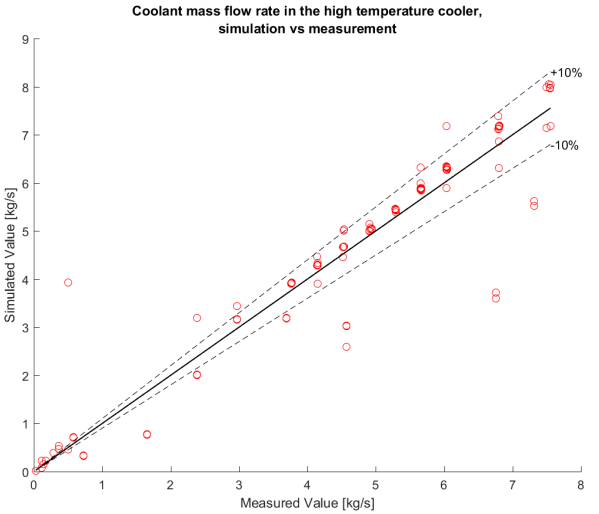

Figure 4.62: Simulation values vs measurement values of the coolant mass flow rate in the high temperature cooler in the steady state cases.

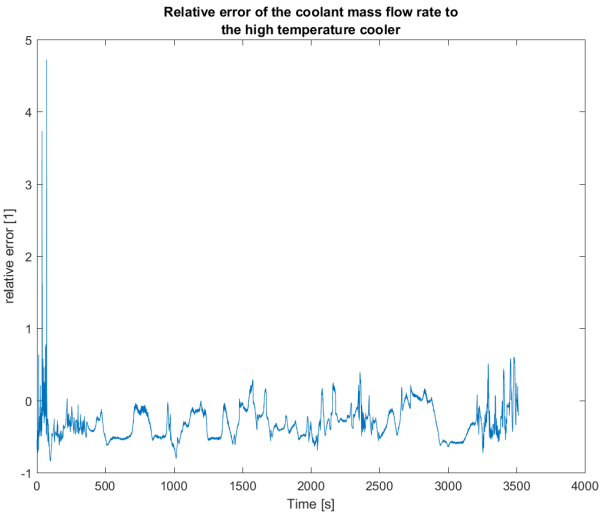

Figure 4.63: Relative error of the coolant mass flow rate through the high temperature cooler in the transient cycle.

4.3 Table Based vs Epsilon Function Heat Exchangers

In the cases studied here, it was found that there was no significant difference between using the epsilon function heat exchanger models rather than the efficiency table based ones, when it comes to computational time. However this should still be taken into account when designing larger systems, as that may have an impact.

The different epsilon function choices for cross flow heat exchangers did not seem to have a large impact on the validity of the system models. However, for further use the epsilon function which describes the heat exchanger best should be used.

4.4 Solver options

The solver selection affected both the translation of the Modelica model and the simulation speed of the model. For the entire cycle model, the original model statistics before translation if shown in Figure 4.64. It shows that it is a very large system with almost 7000 equations.

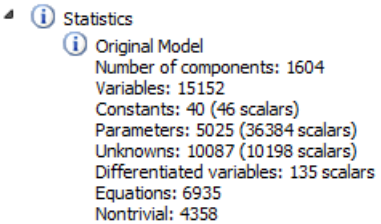

Figure 4.64: Original model statistics

Figures 4.65, 4.66, & 4.67 show the translation statistics of CVODE, explicit Euler, and implicit Euler, respectively. As we can see in all the statistics, before the manipulation there was a large number of large nonlinear systems. The CVODE translation reduced the size of the linear systems, but the translation still had one of size 3. Both the implicit and explicit Euler removed these systems entirely. The nonlinear systems had after manipulation the same sizes for the three solvers. However, the implicit Euler translation had an inlined implicit integration system of size 64, which corresponded to all the coolant components in the cooling cycle model.

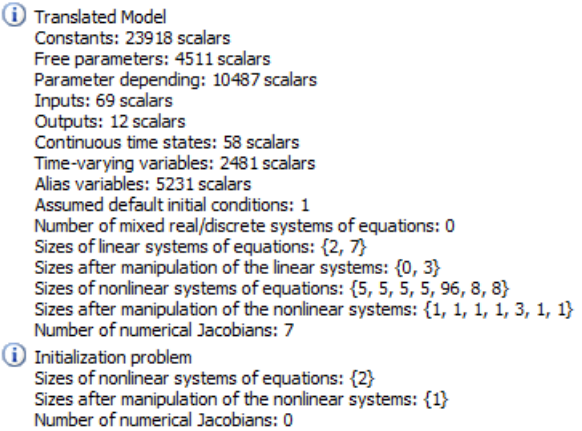

Figure 4.65: Translation statistics of the entire cycle model with CVODE.

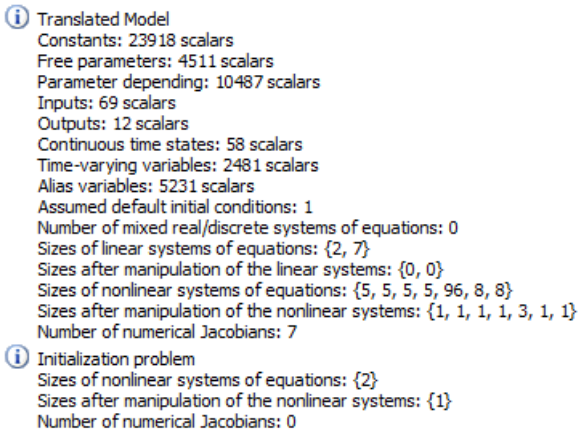

Figure 4.66: Translation statistics of the entire cycle model with explicit Euler

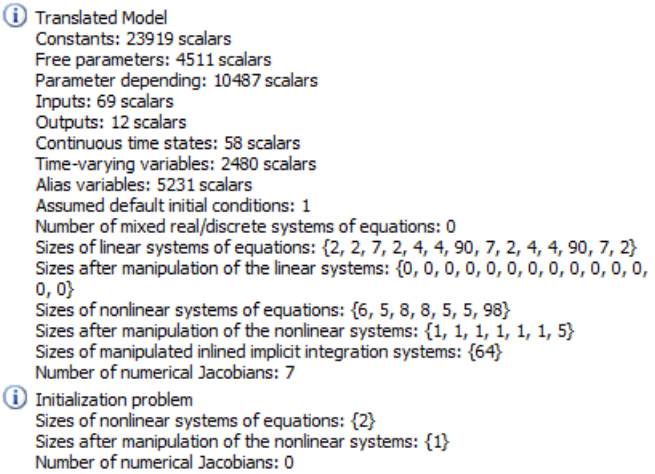

Figure 4.67: Translation statistics of the entire cycle model with implicit Euler

The run time statistics for the simulations of the transient cycle are found in Table 4.1. CVODE was by far the fastest algorithm, clocking in at over 300 times faster than real time. Both the fixed-step algorithms took much longer time, due to requiring more grid points. Explicit Euler could not handle step sizes larger than 10 ms, five times smaller than the real sample time. Implicit Euler however had the capacity to use the real time step size, due to the implicit integration system. This large system was very computationally demanding, and led to the higher CPU-time needed. Both the implicit and the explicit Euler algorithms were faster than real-time, though.

Table 4.1: Run time statistics of the transient cycle with different solvers

Solver	CVODE	Explicit Euler	Implicit Euler
Step size	Variable	0.01 s	0.05 s
CPU-time	15.219 s	199 s	1130 s
Times faster than real time	321	17.66	3.11
CPU-time per interval (0.5 s)	N/A	28.3 ms	161 ms
Time buffer per interval (0.5 s)	N/A	471.7 ms	339 ms

4.5 Optimization

The optimization GUI and scripts developed in MATLAB proved very useful throughout the project. It was mainly used in cases where parameters where un-

known, or simplifications of the actual system needed approximated values.

For example, the retarder model required a pressure drop which in the GT-SUITE model was represented as a series of pressure drops. To simplify the model in Dymola, only one pressure drop component was used, parametrized as was done in Equation 2.3. By setting ζ to an arbitrary value, an initial error time series was generated. Running the optimization algorithm to minimize the error between the simulated values and measured values provided an optimal value for ζ. As is evident in Figure 4.68, the value of the error lies much closer to the y-axis after the optimization.

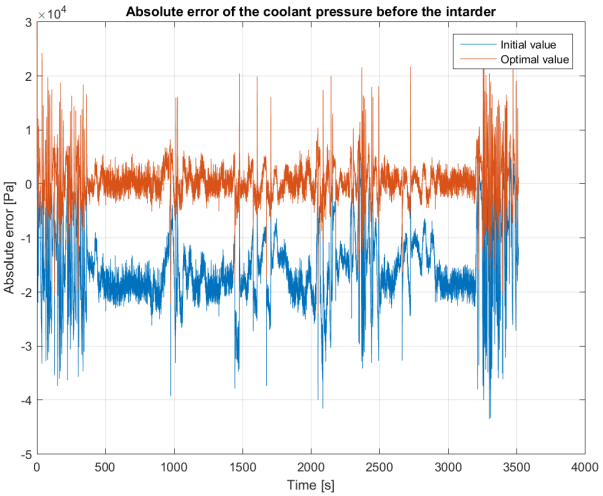

Figure 4.68: Absolute error of the coolant pressure before the intarder, before and after optimization.

4.6 Fix-step solver implementation

The first step towards the real time implementation was to make sure that simulation of the model was possible, with a fix-step integrator with a sufficiently large step size. Two things in particular made this challenging, the flow branching in the coolant system, and the cooling air flow rate in the heat exchanger stack.

The flow branching problem was solved by increasing the flow time constant, which means that some of the dynamics that were too fast for the solver to handle was removed by simplification. As stability and speed was of utmost importance, this change was deemed necessary.

The air flow rate was modeled with pressure boundaries at first, with pressure drops representing the radiator, the heat exchanger stack, the fan, and an extra pressure drop corresponding to the rest of the friction imposed on the flow by the system. This model could not be simulated with a fix-step algorithm, but with CVODE simulation it was possible. This simulation yielded a mass flow rate for the air through the entire system. This mass flow rate was then modeled as a quadratic polynomial of the fan rotational speed and the vehicle speed. By using this approximation, it was possible to simulate the model with similar results with a fix-step algorithm.

4.7 HIL

The dSpace implementation yielded acceptable accuracy and performance. The simulation results were similar to those of Dymola. As for speed, for a step size of 10 ms the average turnaround time was 0.5 ms. This leaves a large amount of time per step and promises possible integration with models of the rest of the power train.

5

Discussion

The purpose of the thesis was to develop a Modelica model of the cooling circuit of one of MAN's long haul truck engines. The model was to be based on existing models and validated with measurement data provided from an actual transient cycle, together with steady state experiments. The requirements on the model were that it had to be fast, accurate, and possible to apply in real time applications.

5.1 Model validity

As seen in Chapter 4, the individual test benches for the components of the cooling system were accurate, regarding both thermodynamical and hydrodynamical properties. These models display the strength in using the efficiency table parametrization when modeling heat exchangers, as the geometrical properties do not have as large of an impact as they have when modeling with with Epsilon-NTU functions.

When looking at the results from the low and high pressure charge air cooler, the air pressure and the heat flow rates of the simulation lie very close to the actual values. The mass flow rates for the coolant are slightly skewed, but this can probably be explained by the fact that the friction model is simplified. Perhaps using a more complex parametrization of the pressure dynamics would lead to closer results, at the cost of higher computational time.

Regarding the heat exchanger stack, the hardest and most time consuming part was creating and assessing the air flow rate model. There were no reliable measurements of the actual flow rate, and no detailed models on the pressure drops present in the flow path. This, combined with the fact that the fixed-step algorithms did not work with only pressure boundary conditions proved a large challenge. At large heat flow rates in the steady state simulation, the simulation values deviated more from the actual values than at lower heat flow rates. These points correspond to those at which the fan speed was higher than average, and as such the air flow rate may not have been properly modeled. A further hindrance with the air flow modeling as a

function of vehicle speed and fan speed, was that during the steady state cases, the vehicle speed was constant over all the states.

In another library from Modelon, the Heat Exchanger Library, there are more detailed heat exchanger models, and stack models in which the air flow can be determined by pressure, and by using that library in the future it is possible to improve accuracy. However, the data provided on the actual cooler was not enough to parametrize such a detailed model during the project.

As for the entire cycle model, the branching flows of the coolant proved to be tricky to model properly. Although the simulated values of the mass flow rates were mostly within $\pm 10\,\%$ of the measured value, deviations in this property propagated to differences in temperature, heat flow rate, etc. However, the cycle model was based on a previously existing model where these deviations in mass flow rate also exist. Given more time, experimenting with different pressure loss coefficients could probably solve this problem.

5.2 Performance

The simulation of the model in Dymola is very fast. It is not only faster than real time using a variable-step solver, but also when using fix step solver, where it runs up to 17 times faster than real time. The speed facilitates model changes and experimenting with parameters, as a simulation run does not take more than a few minutes. It is also integral when applying the model to HIL environment, to keep up with the real time.

6

Conclusions and Future work

6.1 Conclusions

The product of this thesis project is a set of Modelica models developed in Dymola, modeling the components and the cycle which constitutes the liquid cooling system for the engines in MAN's heavy duty trucks. The models are capable of simulating both transient cycles and steady state modes, using fix-step or variable step integration algorithms.

The individual components are based on solid mathematical foundations and have been validated with both transient cycle data and steady state measurement points. In the test benches, the performance is very good, with a few exceptions.

The difficulties with finding a proper model for the cooling air mass flow rate impacted the precision of the heat exchanger stack model, but disregarding that, the stack model behaves as expected and the simulation values lies within ten percent of the actual values at most simulations.

The entire cycle model is able to be simulated and yields acceptable results, regarding the requests from MAN. A point in which the model is lacking is the flow distribution. However, it closely resembles that of the GT simulations, on which the model parametrization was based. The simulation performance is stable, with low simulation time, especially when using the variable step solver CVODE. It is, however, also faster than real time using both the explicit and implicit Euler algorithms, with explicit being the faster one, at the cost of a smaller step size.

Fixed step solver compatibility opens up the possibility for real time applications and HIL-simulations. The exported Simulink steady state model runs fine on the dSpace hardware, and as such a major objective for the project was met.

6.2 Future work

The cycle model lays a foundation for future projects and refinements, a few of which will be listed here.

Improving the air mass flow rate model could have a big impact on the simulation results, especially for the stack model. This could be achieved by actual measurement of the air flow at the engine test bench, or by more accurately modeling the pressure drops occurring in the air flow path. Perhaps utilizing Modelon's Heat Exchanger Library, which contains stack models which can be parametrized and simulated using pressure boundaries, is a possibility. The heat exchanger library also contains finer discretization of the heat exchanger models, and using them may as well lead to better results. However, one must take notice that complex models require more computational power.

Looking at the entire cycle model, it can definitely be improved, either by looking closely at the components and investigate whether they could be simplified, or if they need more complex models to properly capture their dynamics. A starting point could be by modifying the pressure drop components and trying to achieve a flow rate distribution as close to reality as possible.

Currently, the heat flow rate from the internal combustion engine to the liquid cooling system is not modeled, and neither is the heat transfer in the oil cooler and the retarder. Modeling these heat transfer components properly will remove the need for imposing temperature boundary conditions, which would bring the model closer to the goal of being a true closed circuit model for the coolant.

The HIL simulation and interface is not fully developed. After solving the compiling issue, the development may be continued and finished. With functioning HIL models it is possible to integrate the model with other models of the power train to create a unified model of the truck engine systems.

The steady state simulations with dSpace worked well and gave results comparable to the Dymola results. However, it was not tested with the transient cycle and it is possible that the results may not be as good in that case. Continuing the development of the dSpace model and simulating the transient cycle may provide insight in what needs to be done.

Bibliography

[1] J. Batteh, J. Gohl, and S. Chandrasekar. “Integrated vehicle thermal management in modelica: overview and applications”. In: *Proceedings of the 10th International Modelica Conference*. 2014.

[2] T. L. Bergman, A. S. Lavine, F. P. Incropera, and D. P. Dewitt. *Fundamentals of Heat and Mass Transfer*. Seventh edition. John Wiley & Sons, 2011.

[3] *Dymola User Manual Volume 2*. Dassault Systèmes AB. 2016.

[4] H. Elmqvist and S. E. Mattson. “Modelica - the next generation modeling language an international design effort”. In: *Proceedings of the 1st World Congress on System Simulation*. 1997.

[5] *Fundamentals of commercial vehicle technology - Basic information on trucks and buses*. MAN Nutzfahrzeuge Group. 2008.

[6] *Global Optimization Toolbox User’s Guide*. Version 3.4. The MathWorks, Inc. 2016.

[7] *GT-SUITE, General Flow Components Reference Manual*. Gamma Technologies. 2016.

[8] W. M. Kays and A. L. London. *Compact Heat Exchangers*. Third edition. McGraw-Hill, 1984.

[9] *Liquid Cooling Library User’s Guide*. Version 1.5. Modelon. 2016.

[10] B. J. McBride, M. J. Zehe, and S. Gordon. *NASA Glenn Coefficients for Calculating Thermodynamic Properties of Individual Species*. Glenn Research Center, 2002.

[11] Å. Melinder. *Properties of secondary working fluids*. International Institute of Refrigeration, 2010.

[12] D. S. Miller. *Internal Flow Systems*. Second edition. BHRA, 1990.

[13] *TILMedia Add-In for Microsoft Excel*. Version 3.3.1. TLK-Thermo GmbH. 2015.

[14] H. Tummescheit, J. Eborn, and F. J. Wagner. “Development of a modelica base library for modeling of thermo-hydraulic systems”. In: *Modelica Workshop 2000 Proceedings*. 2000.

Lund University
Department of Automatic Control
Box 118
SE-221 00 Lund Sweden

Document name
MASTER´S THESIS

Date of issue
October 2016

Document Number
ISRN LUTFD2/TFRT--6021--SE

Author(s)
Edward Ekstedt

Supervisor
Michael Bernath, MAN Truck & Bus AG
Daniel Andersson, Modelon AB,
Olof Troeng, Dept. of Automatic Control, Lund University, Sweden
Karl-Erik Årzén, Dept. of Automatic Control, Lund University, Sweden
Anders Rantzer, Dept. of Automatic Control, Lund University, Sweden (examiner)

Sponsoring organization

Title and subtitle
Modeling and Simulation of the Cooling System in Heavy Duty Trucks

Abstract

This MSc thesis covers the development of a Modelica model of an engine liquid cooling system for the trucks manufactured by MAN Truck & Bus AG. The mathematical assumptions used for transcribing existing models are described and the reasoning behind the modeling process is provided.

The separate component models are validated with two sets of input signals. Primarily with a dynamic, transient cycle recorded at a testing track. Secondarily, they are also validated with steady state measurements which were part of an experiment conducted at MAN's test bench.

Furthermore, the modeling process of the heat exchanger stack at the front of the vehicle is presented together with points about the boundary conditions of the cooling air. These components are then integrated with each other in a model of the entire cooling system, yielding acceptable simulation results.

Additionally, the simulation performance is evaluated and different integration algorithms are compared and tested, to investigate the possibility of applying the model to real time interfaces. It shows that the model is stable for fixed-step algorithms with small enough step sizes, and that HIL-simulation is possible.

Keywords

Classification system and/or index terms (if any)

Supplementary bibliographical information

ISSN and key title
0280-5316

ISBN

Language
English

Number of pages
1-84

Recipient's notes

Security classification